

# Charged domain walls as quantum strings living on a lattice.

Henk Eskes\*, Osman Yousif Osman, Rob Grimberg, Wim van Saarloos and Jan Zaanen  
*Instituut-Lorentz, Leiden University, P.O. Box 9506, NL-2300 RA Leiden, The Netherlands*  
 (October 19, 2018)

Recently experimental evidence is accumulating that the doped holes in the high- $T_c$  cuprate superconductors form domain walls separating antiferromagnetic domains. These so-called stripes are line-like objects and if these persist in the superconducting state, high- $T_c$  superconductivity is related to a quantum string liquid. In this paper the problem of a single quantum meandering string living on a lattice is considered. A kink model is introduced for the string dynamics which allows us to analyze lattice commensuration aspects. Building on earlier work by den Nijs and Rommelse, this lattice string model can be related both to restricted Solid-on-Solid models, describing the worldsheet of the string in Euclidean space time, and to one-dimensional quantum spin chains. At zero-temperature a strong tendency towards orientational order is found, and the remaining directed string problem can be treated in detail. Quantum delocalized strings are found whose long wavelength wandering fluctuation are described by free field theory, and it is argued that the fact that the critical phase of delocalized lattice strings corresponds to a free Gaussian theory is a very general consequence of the presence of a lattice. In addition, the mapping on the surface problem is exploited to show the existence of new types of localized string phases; some of these are characterized by a proliferation of kinks, but the kink flavors are condensed so that the long wavelength fluctuations of these strings are suppressed. The simplest phase of this kind is equivalent to the incompressible (Haldane) phase of the  $S = 1$  spin chain, and corresponds with a bond centered string: the average string position is centered on bonds. We also find localized phases of this type which take arbitrary orientations relative to the underlying lattice. The possible relevance of these lattice strings for the stripes in cuprates is discussed.

## I. INTRODUCTION

A series of experimental developments has changed the perspective on the problem of high  $T_c$  superconductivity drastically. As long as the doping level is not too high, electrons bind at temperatures well above  $T_c$  [1], and the superconducting state appears to be in tight competition with some collective insulating state [2]. There exists compelling evidence that this insulating state corresponds with a novel type of electron crystal, characterized by both spin- and charge condensation: the stripe phase [3–5]. This phase consists of a regular array of *charged magnetic domain walls*: the holes introduced by doping form line-like textures which are at the same time anti-phase boundaries, separating antiferromagnetic spin domains — see Fig. 1a. This stripe phase is observed in systems where the insulating state is stabilized by Zn doping [5,6] or by the so-called LTT collective pinning potential [3,4].

Inelastic neutron scattering data reveal that strong dynamical stripe correlations persist in the metallic- and superconducting regimes [4,6–8]. Although no static stripe order is present, the magnetic fluctuations as measured by inelastic neutron scattering should reflect stripe correlations. As was shown very recently, the magnetic modulation wavevector of the static stripe phase seems identical with that of the dynamical spin fluctuations in the metal- and superconductor for various doping levels [4].

In addition, it was argued that the anomalous normal state magnetic dynamics can be explained in terms of domain wall meandering dynamics [9].

The exciting possibility arises that the zero temperature superconducting state is at the same time a relatively mildly fluctuating quantum stripe fluid. Unlike the rather featureless diagonal sector of, e.g.,  ${}^4He$  [10], it can be imagined that the charge- and spin sectors of this quantum stripe problem have an interesting internal structure. Because charged domain walls are line-like objects, the charge sector might be looked at as a *quantum string liquid* [9,11,12]. Little is known in general about such problems, and theoretical analysis is needed. In order to address the problem of many interacting strings, it is first necessary to find out the physics of a single string or charged domain wall in isolation. A string is an extended object, carrying a non-trivial collective dynamics — in contrast to particle-like problems, the elementary constituent of the string liquid poses already a serious problem. The physics of quantum strings is a rich subject. This is most easily discussed in terms of path-integrals. In  $D+1$  dimensional Euclidean space time, a particle corresponds with a world line, and so the quantum string corresponds with a “worldsheet”. The statistical physics of membranes is a rich subject, which is still under active investigation [13].

The debate on the microscopic origin of the stripe instability is far from closed [14–18,12,19]. Nevertheless, in

this paper we will attempt to isolate some characteristics which might be common to all present proposals for the microscopy, to arrive at some general considerations regarding the quantum meandering dynamics. From those we will abstract a minimal model for the string dynamics. The phase diagram of this model can be mapped out completely, and turns out to be remarkably rich.

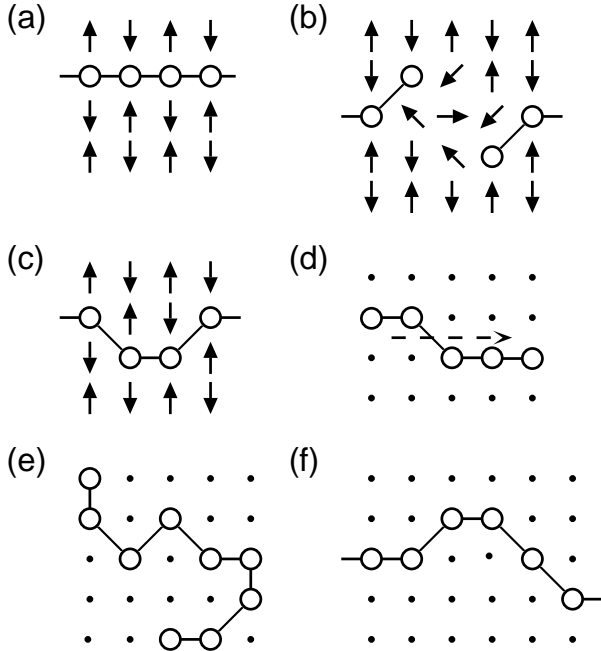


FIG. 1. (a) A charged domain wall separating spin domains of opposite AFM order parameter. (b) Breaking up domain walls causes spin frustration, while (c) “kinks” do not. (d) Kinks can gain kinetic energy by moving along the domain wall. (e) A typical rough wall. (f) An example of a directed string.

These characteristic features are: (i) It is assumed that the charge carriers are confined to domain walls. This is the major limitation of the present work and it is hoped that at least some general characteristics of this strong coupling regime survive in the likely less strongly coupled regime where nature appears to be. (ii) In addition, we assume that domain walls are not broken up, as sketched in Fig. 1b, as this would lead to strong spin frustration. (iii) Most importantly, we assume a dominant role of lattice commensuration on the scale of the lattice constant. Configuration space is built from strings which consist of “holes” which live on the sites of an underlying lattice. An example of such a string configuration is sketched in Fig. 1c. This automatically implies that the microscopic dynamics is that of *kinks* along the string (Figs. 1 c,d), and this leads to major simplifications with regard to the long wavelength behavior of the string as a whole. Note that there is ample evidence for the importance of lattice commensuration: the scaling of the incommensurability with hole density  $x$  for  $x < 1/8$  [6], the special stability

at  $x = 1/8$  [4], the LTT pinning mechanism [3]. (iv) It is assumed that the strings do not carry other low lying internal degrees of freedom, apart from the shape fluctuations. Physically this means that localized strings would be electronic insulators. The data of Yamada *et al.* [5] indicate that this might well be the case at dopings  $x \leq 1/8$  (the linear dependence of the incommensurability on  $x$  indicates an on-domain wall charge commensuration), but it is definitely violated at larger dopings where the strings should be metallic [19–22]. Work is in progress on fluctuating metallic strings, where we find indications that the collective string dynamics is quite similar to what is presented here for insulating strings [23].

Given these requirements, one would like to consider a quantum sine Gordon model [24] for the string dynamics,

$$H = \frac{1}{2} \int dl \left[ \Pi(l)^2 + \frac{1}{c^2} \left( \frac{\delta z(l)}{\delta l} \right)^2 + g \sin \left( \frac{2\pi z(l)}{a} \right) \right]. \quad (1.1)$$

Here  $z(l)$  is the transversal displacement at point  $l$  on the string, and  $\Pi(l)$  its conjugate momentum defined through the commutation relation  $[\Pi(l), z(l')] = i\delta(l - l')$ , and  $c$  is the transversal sound velocity. The first two terms in Eq. (1.1) describe a free string, while the last term is responsible for the lattice commensuration effects: every time the string is displaced by a lattice constant, the potential energy is at a minimum. This model is well understood [24]. When the strength of the nonlinear interaction exceeds a critical value ( $g > g_c$ ), the interaction term is relevant and the string localizes. The excitation spectrum develops a gap and it is characterized by well-defined kink and anti-kink excitations. When  $g < g_c$  the sine term is irrelevant, and although the dynamics is at least initially kink-like on microscopic scales, the string behaves as a free string at long wavelength. The latter is the most elementary of all quantum strings. It follows immediately that the relative transversal displacement of two points separated by an arclength  $l$  along the string diverges as  $\langle (z(l) - z(0))^2 \rangle \sim \ln l$  [9]. The string as a whole is therefore delocalized, and this is the simplest example of a “critical” string.

A central result of this paper is that Eq. (1.1) is, at least in principle, not fully representative for the present lattice problem. More precisely: starting from a more complete microscopic kink dynamics model (section II) we find a richer infrared fixed point structure. The phase diagram incorporates phases associated with the quantum sine Gordon model fixed point, but also includes additional phases which are intimately connected with the effects of the lattice and of the nearest neighbor interactions between the holes. In section III, we derive the path integral representation of our model. It turns out that the worldsheet of this string in Euclidean space time corresponds with two coupled restricted solid-on-solid (RSOS) surfaces [25], each of which describes the

motion of the string in either the  $x$  or  $y$  direction on the two dimensional lattice.

The bare model is invariant under rotations of the string in space. As discussed in section IV, we find indications for a generic zero-temperature spontaneous symmetry breaking: for physical choices of parameters, the invariance under symmetry operations of the lattice is broken. Even when the string is critical (delocalized in space), it acquires a sense of *direction*. On average, the trajectories corresponding with the string configurations move always forward in one direction while the string might delocalize in the other direction, see Fig. 1f. This involves an order-out-of-disorder phenomenon which is relatively easy to understand intuitively. Quantum mechanics effectively enhances the fluctuation dimension by stretching out the string into a world sheet in the time-wise direction, and the enhancement of the effective dimension reduces the effect of fluctuations. Thermal fluctuations destroy this directedness, but they do so more effectively when the string is less quantum mechanical.

This directedness simplifies the remaining problem considerably. We will show that the directed string problem is equivalent to a well known problem in surface statistical physics: its worldsheet is equivalent to a single RSOS surface. At the same time, this model is easily shown to be equivalent to a generalized XXZ quantum spin chain problem. The particular model we study is actually equivalent to the  $S = 1$  spin chain, which has been studied in great detail. The RSOS surface problem and the quantum spin chain problem are therefore also related to each other. This equivalency was actually at the center of the seminal work of den Nijs and Rommelse on the hidden order in Haldane spin chains [26]. From our perspective, the introduction of the physically appealing quantum string model as an intermediate model which connects both with the spin chain and the RSOS surfaces, also helps to appreciate the depth of the work of den Nijs and Rommelse [26].

The bulk of this paper (sections V-VIII) is devoted to an exhaustive treatment of this directed string model. Some powerful statistical physics notions apply directly to the present model, and these allow us to arrive at a complete description of the phase diagram of the quantum string. As was announced already in a short communication [11], this phase diagram is surprisingly rich: there are in total ten distinct phases. In the context of the quantum spin chain/RSOS surfaces, already six of those were previously identified. However, viewing this problem from the perspective of the quantum string, it becomes natural to consider a larger number of potentially relevant operators and the other four phases become obvious.

Compared to strings described by Eq. (1.1), we find a much richer behavior but this is limited to the regime where lattice commensuration dominates over the kinetic

energy so that the string as a whole is localized — we use “localized” here in the sense that the transversal string fluctuations of two widely separated points remain finite,  $\langle (z(\ell) - z(0))^2 \rangle \rightarrow \text{const.}$  as  $\ell \rightarrow \infty$ . Besides the different directions the purely classical strings can take in the lattice, we also find a number of localized strings which have a highly non-trivial internal structures: the “disordered flat” strings, characterized by a proliferation of kinks, but where the kink flavors condense so that the string as a whole remains localized. On the other hand, the quantum-delocalized (critical) strings are all of the free field variety and as we will argue in the final section, this might be a very general consequence of the presence of a lattice cut-off.

## II. MODEL: THE MEANDERING LATTICE STRING

Whatever one thinks about the microscopy of the stripes, in the end any theory will end up considering the charged domain walls as a collection of particles bound to form a connected trajectory, or such a model will be an important ingredient of it. Moreover, these trajectories will communicate with the crystal lattice, because the electrons from which the strings are built do so as well. This fact alone puts some strong constraints on the collective dynamics of the charged domain walls.

Let us consider the string configuration space. On the lattice this will appear as a collection of particles living on lattice sites, while every particle is connected to two other particles via links connecting pairs of sites. The precise microscopic identity of these particles is unimportant: they might be single holes (filled charged domain walls [14,15] as in the nickelates [27]), an electron-hole pair (the charge density waves of Nayak and Wilczek [12], or Zaanen and Oles [18]), or a piece of metallic [20] or even superconducting [28] domain wall. All that matters is that these entities have a preferred position with regard to the underlying lattice (site ordered [14], or bond ordered [19]). Quite generally, curvature will cost potential energy and a classical string will therefore be straight, oriented along one of the high symmetry directions of the lattice. Without loss of generality, it can be assumed that the lattice is a square lattice while the string lies along the  $(1,0)$  ( $'x'$ ) direction. Denoting as  $N_y$  the number of lattice sites in the  $y$  direction and assuming periodic boundary conditions, this straight string can be positioned in  $N_y$  ways on the lattice. Obviously, such a string will delocalize by *local* quantum moves: the particles tunnel from site to site [17,29]. Moving the whole string one position in the  $y$  direction involves an infinity of local moves in the thermodynamic limit, and the different classical strings occupy dynamically disconnected regions of Hilbert space.

This is analogous to what is found in one dimensional systems with a discrete order parameter [30]. In the case of, e.g., polyacetylene the order parameter is of the  $Z_2$  kind: the bond order wave can be either  $\cdots -A-B-A-B-\cdots$  or  $\cdots -B-A-B-A-\cdots$  ( $A$  single bond,  $B$  double bond), while a single translation over the lattice constant transforms the first state of the staggered order parameter into the second kind of state. This is a discrete operation, because the lattice forces the bond-order to localize on the center of the bonds. Such an order parameter structure implies the existence of topological defects, which are Ising domain walls:  $\cdots -A-B-A-B-B-A-B-A-\cdots$  (“kink”) and  $\cdots -B-A-B-A-A-B-A-B-\cdots$  (“antikink”). When they occur in isolated form, these are also genuine building blocks for the quantum dynamics, because although their energy is finite, it involves an infinity of local moves to get rid of them (topological stability). In the particular problem of polyacetylene, these kinks only proliferate under doping (charged solitons). Although topological quantum numbers are no longer strictly obeyed when the density of topological defects is finite, it has been shown in a number of cases that they nevertheless remain genuine ultraviolet quantities as long as they do not overlap too strongly [31,32].

If we consider a (locally) directed piece of string, the string is analogous, except that the symmetry is now  $Z_{N_y}$ : on the torus, a half-infinity of the string is localized at  $y$  position  $n_y$ , and the other half can be displaced to  $n_y + 1, n_y + 2, \dots, n_y - 1$ . Hence, in total there are  $N_y - 1$  distinct kink excitations with the topological invariants corresponding with the net displacement of the half-string in the  $y$  direction. Because the kink operators can occur in many flavors, this problem is therefore in principle richer than that of one dimensional solids.

Clearly, kinks with different flavors have to be dynamically inequivalent. Since there is apparently a reason for the particles to form connected trajectories, it should be more favorable to create a kink corresponding with a small displacement than one corresponding with a large jump. Here we will focus on the simplest possibility: only kinks occur, corresponding with a displacement of *one* lattice constant in the  $y$ -direction. This restriction is physically motivated by the fact that the string is thought to separate two antiferromagnetically ordered states; so, if the displacement of successive holes would be larger than one lattice constant, the antiferromagnetic ordering would be strongly suppressed — after all, this is the very reason that holes tend to line up in stripes. In addition, we will specialize on the “neutral” string. It will be assumed that the string is characterized by a gap in its charge and spin excitation spectrum, so that the strings with kinks contain the same number of particles as the classical reference configurations. The model we will consider might apply literally to the charge commensurate stripes of the nickelate [27]. In the cuprates, it might be

better to consider the stripes as one dimensional metals or superconductors, characterized by massless internal excitations. In these cases, it remains to be demonstrated that eventually the transversal string fluctuations decouple from the internal excitations for the present model to be of relevance.

Given these considerations, we propose the following model for *quantum lattice strings*. The string configurations are completely specified by the positions of the particles (“holes”)  $\mathbf{r}_l = (x_l, y_l)$  on the 2D square lattice. Two successive particles  $l$  and  $l+1$  can only be nearest or next-nearest neighbors, or  $|\mathbf{r}_{l+1} - \mathbf{r}_l| = 1$  or  $\sqrt{2}$ . We will call these connections between successive particles *links*. Two classes of links, those of length 1 and those of length  $\sqrt{2}$ , exist. Taking the order of the particles into account there are 8 distinct links. The string Hilbert space is spanned by all real space configurations satisfying the above string constraint.

We consider local discretized string-tension interactions between nearest and next-nearest holes in the chain, ( $\mathcal{H} = -\beta H$ )

$$\begin{aligned} \mathcal{H}_{Cl} = & \sum_l [\mathcal{K} \delta(|x_{l+1} - x_l| - 1) \delta(|y_{l+1} - y_l| - 1) \\ & + \sum_{i,j=0}^2 \mathcal{L}_{ij} \delta(|x_{l+1} - x_{l-1}| - i) \delta(|y_{l+1} - y_{l-1}| - j)] \\ & + \mathcal{M} \sum_{l,m} \delta(\mathbf{r}_l - \mathbf{r}_m). \end{aligned} \quad (2.1)$$

The various local configurations and interaction energies are shown in Fig. 2. The last term is an excluded volume type interaction — the physically relevant limit is  $M \rightarrow \infty$ , so that holes cannot occupy the same site. The interaction  $\mathcal{K}$  distinguishes horizontal from diagonal links, and  $\mathcal{L}_{ij} = \mathcal{L}_{ji}$  is a set of two-link interactions, which one can think of as microscopic curvature terms. Furthermore, we exclude strings with a physically unrealistic extreme curvature by taking  $\mathcal{L}_{10} \rightarrow \infty$ . Note also that configurations which would give an contribution  $\mathcal{L}_{00}$  to the energy are automatically excluded in the limit  $M \rightarrow \infty$ , which we will take throughout this paper. There are five local configurations, distinguished by four parameters. Therefore we can choose  $\mathcal{L}_{20} = 0$  and the string is determined by the parameters  $\mathcal{K}, \mathcal{L}_{11}, \mathcal{L}_{12}$ , and  $\mathcal{L}_{22}$ , see Fig. 2.

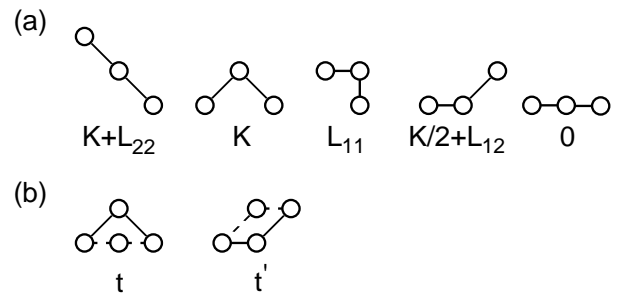


FIG. 2. (a) The set of local configurations and their classical energies. (b) The two allowed hopping processes. We take  $t = t'$ .

The second term in  $\mathcal{H}$  is a quantum term which allows the particles to hop to nearest neighbor lattice positions. However such hopping processes should not violate the string constraint. This constraint can be enforced by means of a projection operator  $P_{Str}(\mathbf{r}_{l+1} - \mathbf{r}_l)$ , that restricts the motion of hole  $l$  to the space of string configurations,

$$P_{Str}(\mathbf{r}) = \delta(|\mathbf{r}| - 1) + \delta(|\mathbf{r}| - \sqrt{2}). \quad (2.2)$$

The string is quantized by introducing conjugate momenta  $\pi_l^\alpha$ ,  $[\pi_l^\alpha, \pi_m^\beta] = i\delta_{l,m}\delta_{\alpha,\beta}$ , where  $\alpha = x$  or  $y$ . A term  $e^{in\pi_l^x}$  acts like a ladder operator, and causes particle  $l$  to hop a distance  $n$  in the  $x$ -direction,

$$e^{in\pi_l^x} |x_l\rangle = |x_l + n\rangle. \quad (2.3)$$

Therefore the kinetic energy term becomes,

$$\mathcal{H}_Q = 2\mathcal{T} \sum_{l,\alpha} P_{Str}^\alpha(\mathbf{r}_{l+1} - \mathbf{r}_l) P_{Str}^\alpha(\mathbf{r}_l - \mathbf{r}_{l-1}) \cos(\pi_l^\alpha). \quad (2.4)$$

Note that the particles, even under  $\mathcal{H}_Q$ , keep their order and therefore can be labeled by  $l$ . Thus the fermion nature of holes in realistic domain walls plays no role at our level of approximation, and quantum statistics becomes irrelevant.

The above model is minimal since it contains only nearest neighbor hopping and the simplest string tension terms. One natural extension would be to take the two hopping amplitudes  $\mathcal{T}$  in Fig. 2b to be different, since there is no microscopic reason why they should be identical. In the next sections we will discuss the zero temperature properties of the above string model. The self-avoidance term is a complicated non-local operator. However, we will find that, surprisingly, the kinetic energy favors *oriented* walls without loops. Therefore this term turns out to be unimportant for the present zero-temperature discussion.

### III. RELATION TO RSOS-LIKE SURFACE MODELS

The problem introduced in the previous section can be reformulated as the classical problem of a two dimensional surface (worldsheet) embedded in 2+1 dimensional space, using the Suzuki-Trotter mapping. The model can be seen as two coupled RSOS (restricted solid-on-solid) surfaces. The solid-on-solid models are classical models for surface roughening [25]. They describe stacks of atoms of integer height in two dimensions, with an interaction between adjacent stacks depending on the height

differences. With this construction overhangs are excluded. In the restricted SOS models these height differences are limited to be smaller or equal to some integer  $n$ . In the present case, the two *RSOS* models parametrize the motions of the world sheet in the spatial  $x$ - and  $y$  directions, respectively, while the (strong) couplings between the two takes care of the integrity of the world sheet as a whole.

In the Suzuki-Trotter [33] or Feynman path integral picture one writes the finite temperature partition function as an infinite product over infinitesimal imaginary time slices. In this limit the commutators between the various terms in the Hamiltonian vanish like  $1/n^2$ , where  $n$  is the number of Trotter slices, and the partition function can be written as,

$$\mathcal{Z} = \lim_{n \rightarrow \infty} Tr \left( e^{\frac{\mathcal{H}_{Cl}}{n}} e^{\frac{\mathcal{H}_Q}{n}} \right)^n. \quad (3.1)$$

To show the relation with RSOS models, we will cast the transfer matrices  $T$  in the form of a two-dimensional classical effective Hamiltonian. This implies writing the matrix elements of the T-matrix between configurations  $\{\mathbf{r}_l\}$  in terms of an effective classical energy depending on the worldsheet positions  $\{\mathbf{r}_{l,k}\}$ , where  $k$  is the imaginary time index running from 1 to  $n$  with periodic boundary conditions. Schematically,

$$\lim_{n \rightarrow \infty} \langle \{\mathbf{r}_l\}_k | e^{\frac{1}{n}\mathcal{H}} | \{\mathbf{r}_l\}_{k+1} \rangle \rightarrow e^{\mathcal{H}_{eff}(\{\mathbf{r}_l\}_k, \{\mathbf{r}_l\}_{k+1})}. \quad (3.2)$$

Since  $\mathcal{H}_{Cl}$  is diagonal in the real-space string basis, it is already in the required form,

$$\lim_{n \rightarrow \infty} \langle \{\mathbf{r}_l\}_k | e^{\frac{1}{n}\mathcal{H}_{Cl}} \rightarrow e^{\frac{1}{n}\mathcal{H}_{Cl}(\{\mathbf{r}_l\}_k)} \langle \{\mathbf{r}_l\}_k |. \quad (3.3)$$

For  $\mathcal{H}_Q$  a few more steps are needed,

$$\begin{aligned} \langle \{\mathbf{r}_l\}_k | e^{\frac{1}{n}\mathcal{H}_Q} | \{\mathbf{r}_l\}_{k+1} \rangle &= \langle \{\mathbf{r}_l\}_k | \sum_{m=0}^{\infty} \frac{1}{m!} \left( \frac{\mathcal{H}_Q}{n} \right)^m | \{\mathbf{r}_l\}_{k+1} \rangle \\ &= \langle \{\mathbf{r}_l\}_k | 1 + \frac{\mathcal{H}_Q}{n} | \{\mathbf{r}_l\}_{k+1} \rangle + \mathcal{O}(\frac{1}{n^2}) \\ &= \prod_l \prod_{\alpha=x,y} (\delta(\alpha_{l,k+1} - \alpha_{l,k}) \\ &\quad + \frac{\mathcal{T}}{n} \delta(|\alpha_{l,k+1} - \alpha_{l,k}| - 1)) \\ &= e^{\sum_l \ln(\frac{\mathcal{T}}{n}) [\delta(|x_{l,k+1} - x_{l,k}| - 1) + \delta(|y_{l,k+1} - y_{l,k}| - 1)]}. \end{aligned} \quad (3.4)$$

The expression in the last line is of course only valid for states in which the  $\alpha_l$ 's in successive time slices differ by at most one unit. Combining these two energy contributions we arrive at the following classical problem,

$$\begin{aligned}
\mathcal{Z} &= \lim_{n \rightarrow \infty} \text{Tr} e^{\mathcal{H}_{\text{eff}}} \\
\mathcal{H}_{\text{eff}} &= \sum_{l,k} \left[ \frac{\mathcal{K}}{n} \delta(|x_{l+1,k} - x_{l,k}| - 1) \delta(|y_{l+1,k} - y_{l,k}| - 1) \right. \\
&+ \sum_{i,j=0}^2 \frac{\mathcal{L}_{ij}}{n} \delta(|x_{l+1,k} - x_{l-1,k}| - i) \delta(|y_{l+1,k} - y_{l-1,k}| - j) \\
&+ \frac{M}{n} \sum_m \delta(x_{l,k} - x_{m,k}) \delta(y_{l,k} - y_{m,k}) \\
&+ \ln\left(\frac{\mathcal{T}}{n}\right) [\delta(|x_{l,k+1} - x_{l,k}| - 1) \\
&\quad \left. + \delta(|y_{l,k+1} - y_{l,k}| - 1)] \right]. \quad (3.5)
\end{aligned}$$

This classical world sheet is constrained to  $|x_{l,k+1} - x_{l,k}| \leq 1$  and  $|y_{l,k+1} - y_{l,k}| \leq 1$ , and the interactions are anisotropic. The above classical model can be viewed as two coupled two-dimensional RSOS surfaces,  $x_{l,k}$  and  $y_{l,k}$ . The  $x$  coordinate of hole  $l$  at the time slice  $k$  is now identified as the height of an RSOS column positioned at  $(l, k)$  in the square lattice. In a similar way the  $y$  coordinates define a second RSOS surface, coupled strongly to the first by the above classical interactions. Since the steps  $\Delta x$  can at most be equal to 1, the RSOS sheets are restricted to height differences 0,  $\pm 1$  between neighboring columns.

The classical model as defined above is not unique. While the above mapping allows us to exploit the connection to other models most efficiently, for the numerical Monte-Carlo calculations a different decomposition is used, which allows for a more efficient approach to the time continuum limit. We write,

$$\begin{aligned}
\mathcal{Z} &= \text{Tr} e^{\mathcal{H}_{Cl} + \mathcal{H}_Q} \\
&= \lim_{n \rightarrow \infty} \text{Tr} (I T_A I T_B)^n. \quad (3.6)
\end{aligned}$$

In the above formula  $I$  is the identity operator, in our case a complete set of string configurations. We have chosen to split the  $T$ -matrix into a contribution from even and odd sites, or A and B sublattice (checkerboard decomposition),

$$T_A = \exp \left[ \frac{1}{n} \sum_{l=1}^{L/2} (\mathcal{H}_{Cl,2l} + \mathcal{H}_{Q,2l}) \right], \quad (3.7)$$

and a similar expression for the odd sites.  $\mathcal{H}(2l)$  is the Hamiltonian of the even string element  $2l$ , equal to Eq. (2.1) or (2.4) without the sum over string links.  $L$  is the number of links in the chain. Because of the sublattice decomposition,  $T_A$  is a simple product of local T-matrices and  $\mathcal{Z}$  becomes,

$$\begin{aligned}
\mathcal{Z} &= \lim_{n \rightarrow \infty} \sum_{\{\mathbf{r}_{l,k}, \mathbf{r}'_{l,k}\}} \prod_{k=1}^n \prod_{l=1}^{L/2} \langle \{\mathbf{r}_l\}_k | t_A^{2l,k} | \{\mathbf{r}_l\}'_k \rangle \\
&\quad \langle \{\mathbf{r}_l\}'_k | t_B^{2l+1,k} | \{\mathbf{r}_l\}_{k+1} \rangle. \quad (3.8)
\end{aligned}$$

Each timeslice is split in two subslices,  $\mathbf{r}$  and  $\mathbf{r}'$ . The notation  $\{\mathbf{r}_l\}_k$  denotes the set of positions  $\mathbf{r}_l$  at the given time slice with index  $k$ . Note that the  $t$  matrices are independent of  $l$  and  $k$ , and these indices only label the position of the  $t$  matrix in the 2D world sheet. The local  $t$  matrices,  $t_A$  and  $t_B$ , depend only on three positions. For instance,

$$\begin{aligned}
\langle \{\mathbf{r}_l\}_k | t_A^{2l,k} | \{\mathbf{r}_l\}'_k \rangle \\
= \langle \mathbf{r}_{2l-1,k} \mathbf{r}_{2l,k} \mathbf{r}_{2l+1,k} | t_A^{2l,k} | \mathbf{r}'_{2l-1,k} \mathbf{r}'_{2l,k} \mathbf{r}'_{2l+1,k} \rangle \quad (3.9)
\end{aligned}$$

with the restriction  $\mathbf{r}_{2l-1,k} = \mathbf{r}'_{2l-1,k}$  and  $\mathbf{r}_{2l+1,k} = \mathbf{r}'_{2l+1,k}$ . Since each link has 8 different orientations, the local  $t$  matrix connects in general  $8 \times 8 = 64$  possibilities. However most of the  $t$  matrix elements are zero, and it decomposes into subblocks, of which the biggest one is  $3 \times 3$ . The states which are connected via the local  $t$  matrix, or the Hamiltonian, are listed in Fig. 3, and the matrix elements are given in the appendix. The above decomposition will be used in the Monte-Carlo simulations described in Section IV.

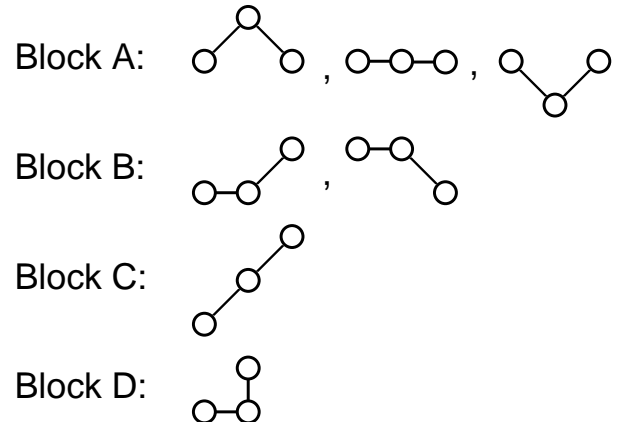


FIG. 3. The four subblocks of the local  $t$ -matrix. The other equivalent, symmetry related blocks are obtained by  $\pi/2$  rotations and reflections in the  $x$  or  $y$  axis.

#### IV. DIRECTEDNESS AS SPONTANEOUS SYMMETRY BREAKING

We are not aware of any similarity of the statistical physics problem of the previous section with any existing model. RSOS problems are well understood, but it should be realized that in the present model the two RSOS problems are strongly coupled, defining a novel dynamical problem. When we studied this problem with quantum Monte-Carlo, we found a generic zero temperature symmetry breaking: although the string can be quantum delocalized, it picks spontaneously a *direction* in space. This symmetry breaking happens always in the part of parameter space which is of physical relevance.

Our understanding of this phenomenon is a nice illustration of an order-out-of-disorder mechanism which at first sight appears paradoxical, but which is easy to understand qualitatively. At first sight, one might expect that the quantum fluctuations (kinetic energy) would tend to disorder a string, i.e., to decrease the tendency for the string to be directed. That the opposite effect happens, is due to the fact that in the presence of quantum fluctuations, the string traces out a worldsheet in the imaginary time direction. The larger the kinetic term, or the larger the temperature, the further the worldsheet stretches out in the timewise direction. At zero temperature, the worldsheet becomes infinite in this direction as well. The statistical physics of a string is then equivalent to that of a fluctuating sheet in three dimensions. Now, it is well known from studies of classical interfaces [34] that while a one-dimensional classical interface in two dimensions does not stay directed due to the strong fluctuations, for a two-dimensional sheet the entropic fluctuations are so small that interfaces can stay macroscopically flat in the presence of a lattice [35,36] — for this reason, the roughening transition in a three-dimensional Ising model is properly described by (i.e., is in the same universality class as) a Solid-on-Solid model in which overhangs are neglected [35,36]. In other words, even if microscopic configurations with overhangs are allowed, a classical interface on a lattice in three dimensions can stay macroscopically flat or “directed”. In agreement with this picture, we will find that the directedness order becomes more robust when the string quantum-fluctuations become more severe, i.e., when the worldsheet stretches out further into the timewise direction.

It is convenient to use open spatial boundary conditions. In this case, the string configuration space of the model defined in section II consists of all surfaces, connecting to the boundaries in the space-directions while periodic along the imaginary time direction. On a time slice, the trajectories can be categorized according to the global property of *directedness*: when the string connects two opposite sides of the lattice in the spatial directions, this trajectory can be called “directed” and otherwise it is undirected. An alternative, more restrictive definition of directedness is: every continuous string configuration  $s$  can be written as a parametrized curve in two dimensions,  $[x(t), y(t)]$ , where  $t$  could for instance be the discrete label of the successive particles along the string. When the string configuration can be parametrized by a single-valued function  $x(y)$  or  $y(x)$ , we call the string configuration directed (see Fig. 1f). The quantum string vacuum is a linear superposition of many string configurations. When all configurations in the vacuum correspond with single valued functions  $x(y)$  or  $y(x)$ , the string vacuum has a directedness order parameter. We will give an explicit measure of the directedness in our simulations below.

It should be immediately clear that directedness or-

der is rather fragile. *It cannot exist at any finite temperature.* When temperature is finite, the width of the worldsheet in the imaginary time direction becomes finite as well, and the long wavelength fluctuations of the string becomes a 1D statistical problem, subjected to string boundary conditions which are inconsequential for the argument which follows. Consider first the classical limit: at zero temperature the string would be straight, running along (say) a  $(1,0)$  direction. A local ‘corner’ configuration of the type shown in Fig. 2a would be an excitation with energy  $L_{11}$  (alternatively, one could consider two kinks). Clearly, a single corner suffices to destroy the directedness of the classical ground state. At any finite temperature, the probability of the occurrence of at least one corner is finite:  $P = N \exp(-\beta L_{11})$ . Hence, directedness order cannot exist at finite temperatures, for the same reasons that long range order is destroyed at any non-zero temperature in one dimension.

At zero temperature, the internal dynamics of the worldsheet is that of a two-dimensional sheet which is infinite in both directions and since the lattice commensuration has rendered the problem to be of a discrete symmetry, long range order can exist for finite kinetic energy. We will discuss the symmetry breakings of a single RSOS surface in great detail later. For the present discussion it suffices to know that such a single RSOS surface can be fully ordered, as well as (partly) disordered. Because of the strong coupling, it would a priori appear questionable to discuss the dynamics of the full model of Section II in terms of the dynamics of the two separate RSOS subproblems. However, in the context of directedness it is quite convenient to do so. When both the  $x$  and  $y$  RSOS problems would be fully disordered, it is easy to see that the string vacuum would be undirected. This is illustrated in Fig. 4a: two kinks moving the string from a  $(1,0)$  to a  $(0,1)$  direction in the lattice correspond with one kink which can move freely in the horizontal part of the string, and one kink which can move freely in the vertical part of the string. On the other hand, when both RSOS problems are ordered, the string is also ordered. For instance, the  $(1,0)$  string can be thought of as a combination of an RSOS surface which always steps upwards in the  $x$  direction, and one which is horizontal in the  $y$  direction (Fig. 4b).

A third possibility is that one of the RSOS subproblems is ordered, while the other is disordered. Dismissing crumpled phases (like condensates of the  $L_{11}$  type corners), the only possibility remaining is that one of the RSOS problems steps up always, while the other is disordered, as illustrated in Fig. 4c. This results in a disordered *directed* string vacuum: the string steps always forward in, say, the  $x$  direction while it freely fluctuates in the  $y$  direction. We find that this symmetry breaking happens *always* as long as the string does not crumple.

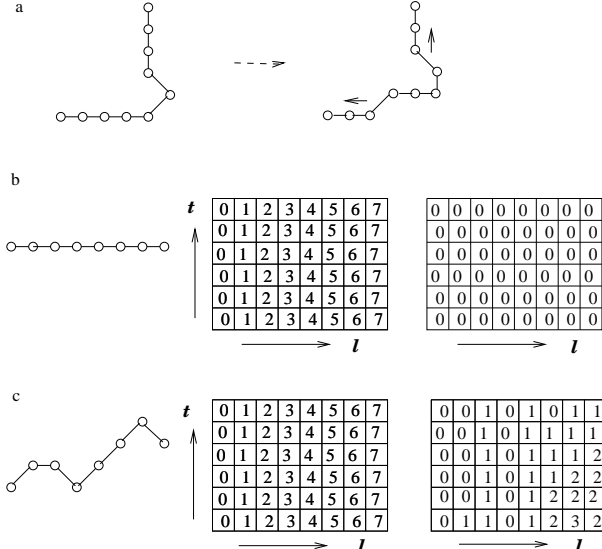


FIG. 4. (a) An undirected string with two kinks propagating along different directions. Note that the bend blocks the propagation of kinks. (b) a (1,0) string and the corresponding two (coupled) RSOS surfaces along the  $x$  and the  $y$  directions respectively. The numbers correspond to  $x$  ( $y$ ) position of hole  $l$  at imaginary time  $t$ . (c) a disordered *directed* string and the corresponding ordered and disordered RSOS surfaces

To perform Monte-Carlo calculations on the string model, we used the checkerboard decomposition as described in Sec. III. Note that the string has no minus sign problem — the sign of  $\mathcal{T}$  is easily transformed away by an appropriate choice of the operators. For  $\mathcal{L}_{10} \rightarrow \infty$ , there are  $8 \times 5 = 40$  different local configurations, given by the positions  $\mathbf{r}_{l-1}$ ,  $\mathbf{r}_l$  and  $\mathbf{r}_{l+1}$ . However most of the  $40 \times 40$  local  $T$  matrix elements are zero, and the largest subblock is  $3 \times 3$ . These blocks were listed in Fig. 3. The corresponding matrix elements are listed in the appendix. For the Monte-Carlo program to produce sensible results it is crucial to have operations that add and remove bends easily. We added global mirror and  $\pi/2$  rotation operations illustrated in Fig. 5.

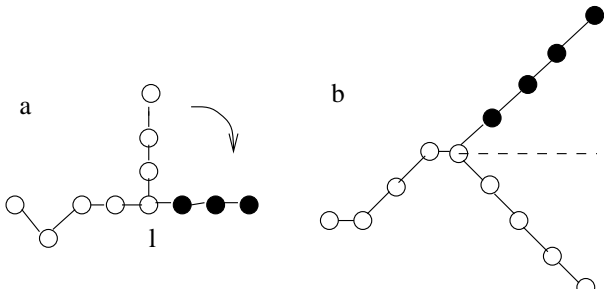


FIG. 5. Two additional Monte Carlo operations used for the simulations of the general string. The 90 degree rotation (a) around position 1 in this example turns a non-directed string into a directed one. The mirror operation (b) is important to quench defects in diagonal strings (mirror plane indicated by the dashed line).

In the latter case half of the string is rotated around any of the sites  $l \in 2..L-1$ . This means that for instance the position of all holes  $m > l$  are replaced by  $(x_m, y_m) \rightarrow (x_l, y_l) + (y_m - y_l, -(x_m - x_l))$ . Such operations turn out to be very efficient — completely wrapped high temperature strings unwrap in just a couple of Monte Carlo steps at low temperature.

We discovered this directedness symmetry breaking during the simulations. To quantify the directedness we measured the fraction of string length in the string vacuum corresponding with single valued configurations. At zero temperature, the ground state wave function of the string is,

$$|\Psi_0\rangle = \sum_{\{x_l, y_l\}} \alpha_0(\{x_l, y_l\}) |\{x_l, y_l\}\rangle. \quad (4.1)$$

where every state in string configuration space ( $|\{x_l, y_l\}\rangle$ ) corresponds with a trajectory  $[x(t), y(t)]$ . Consider first the case of a continuous string. For every configuration, the total string arclength is given by

$$L(\{x_l, y_l\})_{tot} = \int ds = \int \sqrt{dx^2 + dy^2}. \quad (4.2)$$

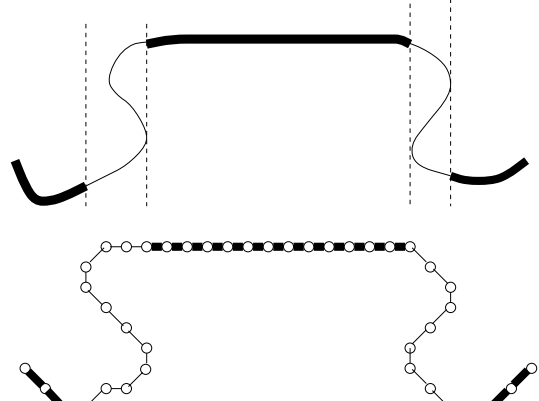


FIG. 6. Illustration of the way we measure the directedness of a string in the continuum case (a) and on the lattice (b). The heavy solid parts of the string indicate the parts where the projection of the string onto the  $x$  axis is single-valued, and for which the indicator function  $g_y(x)$  equals 1.

To quantify the directedness, we introduce, as illustrated in Fig. 6, an indicator function  $g_y(x)$  which equals 1 when the string is single-valued when projected onto the  $x$ -axis, and zero otherwise, and analogously a function  $g_x(y)$  which equals 1 when the curve is single-valued when projected onto the  $y$ -axis, and zero otherwise. The total directed length in the  $x$  and  $y$  directions are then defined as

$$L(\{x_l, y_l\})_{dir,x} = \int dx g_y(x) \sqrt{1 + \left(\frac{dy}{dx}\right)^2},$$

$$L(\{x_l, y_l\})_{dir,y} = \int dy g_x(y) \sqrt{1 + \left(\frac{dx}{dy}\right)^2}. \quad (4.3)$$

The measure of directedness in the string vacuum is then defined as the larger of  $N_{dir}^x(0)$  and  $N_{dir}^y(0)$ , where

$$N_{dir}^\eta(0) = \sum_{\{x_l, y_l\}} |\alpha^0(\{x_l, y_l\})|^2 \frac{L(\{x_l, y_l\})_{dir,\eta}}{L(x_l, y_l)_{tot}}, \quad (4.4)$$

where  $\eta = x, y$ . On the lattice, our measure of directedness is the immediate analogue of this definition, except that we just count the number of directed bonds, irrespective of whether they are oriented diagonally or horizontally.

By thermal averaging, the above definition of directedness density is immediately extended to finite temperature,

$$N_{dir}^\eta(T) = \sum_n e^{-\beta(E_n - E_0)} N_{dir}^\eta(n), \quad (4.5)$$

where  $N_{dir}^\eta(n)$  is the directedness density of a string excitation with energy  $E_n$ . Eq. (4.5) can be straightforwardly calculated using quantum Monte-Carlo. A Monte-Carlo snapshot defines a stack of coupled string configurations along the imaginary time direction (the Trotter direction). We calculate  $N_{dir}^x$  for every Trotter slice by calculating the fraction of the string length in this configuration which is single valued in the  $x$ -direction. This is given by the number of bonds which steps forward in the  $x$ -direction devided by the total number of bonds in the string. We then average this quantity over the string world sheet (Trotter direction) and then over the Monte-Carlo measurements. The same is done for  $N_{dir}^y(n)$ . The larger of  $N_{dir}^x(n)$  and  $N_{dir}^y(n)$  is then the density of directedness at the given temperature.

That the zero-temperature properties of the directed and non-directed string are equivalent for  $\mathcal{L}_{11} \geq 0$  can be understood by the following argument. The  $\pi/2$  bends in strings block the propagation of links along the chain. Close to the bend itself the particles in the chain cannot move as freely as in the rest of the chain. This effect is shown in Fig. 7.

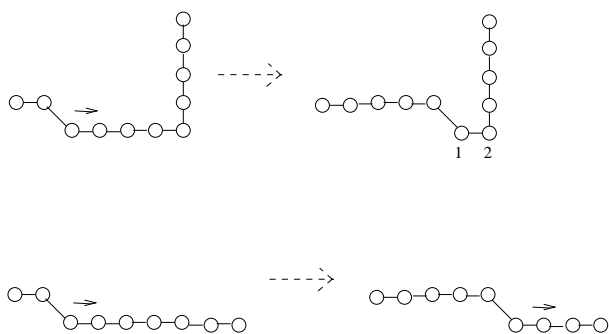


FIG. 7. Illustration of the fact that a bend blocks the propagation of links along the string. Note holes 1 and 2 cannot move.

In space-time the  $\pi/2$  bend is like a straight rod in time. Therefore the presence of such kinks increase the kinetic energy. For the argument it makes little difference whether the bend consists of a single  $\pi/2$  corner or two  $\pi/4$  corners. This confirms that *it is the kinetic energy which keeps the strings oriented along one particular direction*. In terms of a directedness order parameter this result implies that such a quantity is always finite, except when  $\mathcal{L}_{11} \ll 0$  or when the hopping term vanishes (it is easy to see that in the classical case,  $\mathcal{T} = 0$ , in many regions of parameter space the problem becomes that of a self-avoiding walk on a lattice in the limit  $T \rightarrow 0$ ). For the two equivalent RSOS surfaces this means that one of the two spontaneously orders and becomes diagonal, while the other RSOS sheet shows any of the ten quantum rough or classically ordered phases discussed later.

In Fig. 8 we show results of typical Monte-Carlo calculations for the density of directedness as a function of temperature  $N_{dir}(T)$ . We have considered four points in the parameters space; as will be discussed later, these points are representative for phases with interesting quantum fluctuations, and serve to clarify our conclusion. In Fig. 8(a) the triangles (dashed line) is the result for the density of directedness at the point where all the classical curvature energies are zero, i.e., corresponding to the pure quantum string. The crosses (dotted line) and the filled squares (dashed-dotted line) are the results for points where  $\mathcal{K} = 1.8$  and  $\mathcal{K} = 4.0$  respectively, and the rest of the classical curvature energies are zero. In term of the phase diagram for the directed string problem of Fig. 11 in section VI and Table III in section VII, the first point corresponds to a Gaussian string (pure quantum) and the other two correspond to flat strings. The point  $\mathcal{K} = 1.8$  lies just inside the flat string phase II where significant quantum fluctuations are still present, while the point  $\mathcal{K} = 4.0$  lies deep inside the flat phase. The fourth curve in Fig. 8(a), given by the full line, is the result of a Monte-Carlo calculation for a classical string ( $\mathcal{T} = 0$ ) where only flat segments and  $\pi/2$  corners are allowed (no diagonal segments). This same classical result is shown again in Fig. 8(b) together with the result of the directedness density for a point in the middle of the Gaussian (XY) phase [ $\mathcal{K} = 0.5$ ,  $\mathcal{L}_{21} = -0.25$ ,  $\mathcal{L}_{22} = -1.0$ ,  $\mathcal{L}_{11} = 0$  corresponding to  $D = 0$  and  $J = -0.5$ ].

We will first discuss the result for the classical case, a classical string ( $\mathcal{T} = 0$ ) with  $\mathcal{L}_{11}$ , the energy of the  $\pi/2$  corner, equal to one. Because the string is of finite length, the infinite temperature limit of  $N_{dir}(T)$  is not zero but rather a small but nonzero value [37] ( $\sim 0.03$  for a domain wall of length 50).  $N_{dir}(T)$  is already close to this value for all temperatures of order  $\mathcal{L}_{11}$  and larger. For an infinitely long domain wall  $N_{dir}(T)$  drops very fast to zero with increasing temperature. At the other limit, for low  $T$  where  $T \ll \mathcal{L}_{11}$ ,  $N_{dir}(T)$  grows very fast to 1.

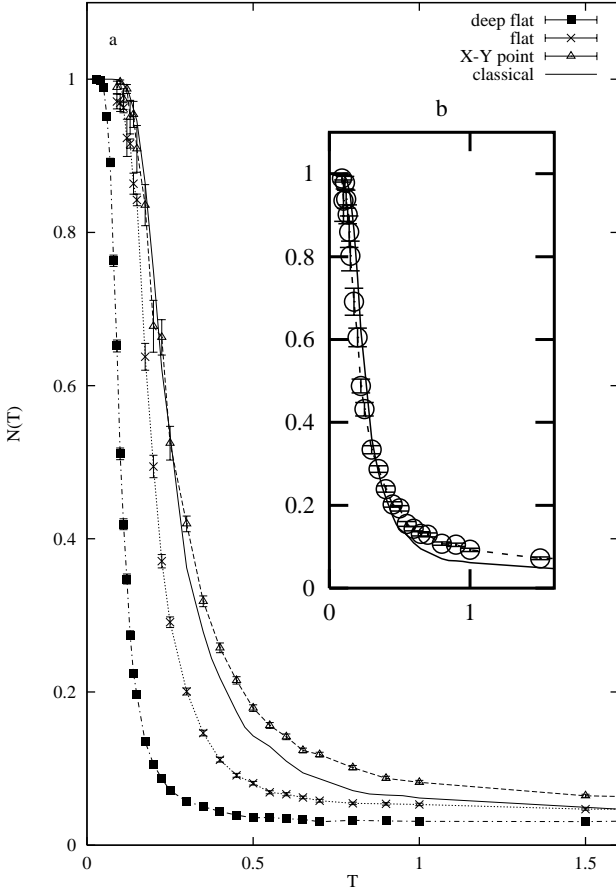


FIG. 8. A Monte-Carlo result for the directedness density  $N_{dir}(T)$  at 4 points. (a) The XY point (Triangles) where all curvature energies are zero. Two points in the flat phase, with  $\mathcal{K} = 1.8$  (crosses) and  $\mathcal{K} = 4.0$  (filled squares) the rest of the curvature energies are zero. (b) Inset: A point in the middle of the gaussian phase with parameters  $\mathcal{K} = 0.5$ ,  $\mathcal{L}_{21} = -0.25$ ,  $\mathcal{L}_{22} = -1.0$ ,  $\mathcal{L}_{11} = 0$  (open circles). The full line in both figures is the result for a classical string where only flat bonds and  $\frac{\pi}{2}$  corners are present with  $\mathcal{L}_{11} = 1$ .

Again because the string is of finite length, it becomes directed already at a finite temperature: For all temperatures such that  $L \exp(-\beta \mathcal{L}_{11}) < 1$  the string configurations in our simulations are typically completely directed. An infinitely long classical string becomes directed only at  $T = 0$ , of course, since at any nonzero temperature always some corners will occur in a sufficiently long string.

For the quantum string, all the curves look strikingly similar to the classical one. When the temperature is very much higher than the kinetic term,  $T \gg \mathcal{T}$ , all curves merge together and the classical limit is reached. At low  $T$ , where  $T \ll \mathcal{T}$ ,  $N_{dir}(T)$  again grows very fast to 1, as in the classical case; it reaches this value at a finite temperature for the finite length string. This is even true for the purely quantum string at the XY point, where all classical microscopic curvature energies are zero (see the dashed line in Fig. 8(a)). We can understand this in terms of an effective corner or bend energy  $\bar{\mathcal{L}}$  that is

produced by the quantum fluctuations. As in the classical case the probability for the occurrence of a bend is proportional to  $\sim \exp(-\beta \bar{\mathcal{L}})$ . At zero temperature no bend is present and the string becomes directed. A finite length string effectively becomes directed already at a temperature such that  $L \exp(-\beta \bar{\mathcal{L}}) < 1$ . At intermediate temperatures, where the temperature is of the order of the kinetic term, things are more difficult and it is far from obvious what is going on. Especially in this region, all the various classical curvature energies may play a role, and the interplay of these on the directedness is unclear. Nevertheless, as is clear from the data of Fig. 8(a), this region connects the high and low temperature limits smoothly. Moreover, by comparing the results for the three quantum strings in this figure it is also clear that when the string is more quantum mechanical  $N_{dir}(T)$  is higher.

Our general conclusion, based also on Monte-Carlo studies of the behavior in other phases which are briefly summarized below, is that *apart from some extreme classical limits, the general lattice string model at zero temperatures is a directed string*. The qualitative picture of  $\pi/2$  turns blocking the propagation of kinks appears to be a natural explanation for these Monte-Carlo findings. The phase diagram of the general string model introduced in section II will essentially be the same (apart from special limits) as the corresponding phase diagram of the simplified directed string model. In the remaining sections of this paper we will therefore focus on the phases and phase transitions of the directed string.

For completeness, we end this section with a brief qualitative description of our observations concerning spontaneous directedness at low but finite temperatures in regions of the phase diagram where the directed string has other type of ordering than that already discussed. All the results apply to  $\mathcal{L}_{11} = 0$ , and we refer to Table III in section VII for a quick introduction to the various phases of the directed string problem and for the numbering (I–X) of the various phases.

— The entire zero temperature phase diagram of the directed string is reproduced.

— Phase I is very stable with respect to bends. With “stable” we mean that *finite* strings do not change their appearance when increasing the temperature from zero to a moderately small temperature, of the order of  $0.1 \mathcal{T}$ .

— Deep in the horizontal phase II (large positive  $\mathcal{K}$ ) quantum fluctuations are strongly suppressed, and at the same time the string becomes susceptible to  $\pi/2$  corners. On the other hand, when we approach from phase II the boundaries with phases IV and V, the fluctuations increase and the string stiffens, Fig. 8. This is in agreement with the picture sketched before that quantum fluctuations orient the string.

— Deep inside phase III the string changes constantly between horizontal zigzags and vertical zigzags. A  $\pi/2$  turn costs no extra energy. Again close to phase V quan-

tum fluctuations have the effect of removing bends.

— The Haldane phase V and the rough phase IV are very robust, and a considerable fraction of  $\pi/2$  bends occurs only at relatively high temperatures of the order of  $0.2\mathcal{T}$ .

— In the slanted phase VII high temperatures are needed before down diagonal links come in. On the other hand horizontal links are easily replaced by vertical ones. This only increases the energy very slightly, but the entropy gain is considerable. A typical low temperature string is shown in Fig. 9 in section VII. To zeroth order the horizontal and vertical links can be thought of as spinless fermions moving coherently along the string. In the dilute limit these links have only a weak interaction. The order of the links is conserved, and at zero temperature the ground state has only horizontal links. However our simulations indicate that for a small range of negative  $L_{11}$  values a diagonal string with alternating horizontal and vertical links is favoured. It is again the kinetic energy of the horizontal and vertical links that keeps the string oriented in the (1,1) direction.

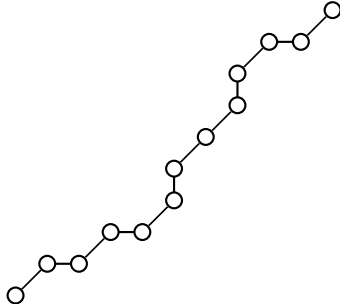


FIG. 9. A typical low temperature string in the slanted parameter region VII.

## V. DIRECTED STRINGS AND THE SPIN-1 CHAIN

Quite generally, the string problem does not simply reduce to that of the internal dynamics of the worldsheet, because of the requirement that the worldsheet has to be embedded in  $D+1$  dimensional space. However, in the presence of directedness order and in the absence of particle number fluctuations [21] the string boundary conditions are trivially fulfilled and the string problem is equivalent to that of a single “world sheet” in 1+1 dimensions. Assume the string to be directed along the  $x$  direction. Since the string steps always forward in this direction, the number of particles in the string has to be equal to the number of lattice sites in the  $x$ -direction, and every directed string configuration will connect the boundaries in this direction. The string is still free to move along the  $y$  direction. Instead of labeling the positions in the 2D plane the string is completely specified by the list of links, for which there are only 3 possibilities (in the (1,1), (1,0), or (1,-1) direction), and the

position of a single “guider point”. As a guider point we can take the position  $\mathbf{r}$  of any one of the particles, which, together with the relative coordinates given by the links, fixes the position of the entire string. Since the guider represents just a single degree of freedom, and since the thermodynamic behavior of a chain is determined by the link interactions, the guider coordinates will be irrelevant for the behavior of the chain. Apart from this guider degree of freedom the directed string problem reduces to a one-dimensional quantum problem with three flavors.

From Eq. (3.5) one directly deduces the Hamiltonian of the string directed along  $x$ ,

$$\begin{aligned} \mathcal{H}_{eff} = \sum_{l,k} \left[ & \frac{\mathcal{K}}{n} \delta(|y_{l+1,k} - y_{l,k}| - 1) \right. \\ & + \frac{\mathcal{L}_{12}}{n} \delta(|y_{l+1,k} - y_{l-1,k}| - 1) \\ & + \frac{\mathcal{L}_{22}}{n} \delta(|y_{l+1,k} - y_{l-1,k}| - 2) \\ & \left. + \ln\left(\frac{\mathcal{T}}{n}\right) \delta(|y_{l,k} - y_{l,k+1}| - 1) \right]. \end{aligned} \quad (5.1)$$

It is clear that the directedness simplifies the model considerable. The directed version can not self-intersect, and the excluded volume constraint is satisfied automatically. Furthermore the  $\mathcal{L}_{11}$ -type of configurations are not allowed, thus the directed model is specified by three parameters and the temperature ( $\mathcal{T} = 1$ ). Because of the preceding considerations, Eq. (5.1) corresponds with a 1+1 D problem, which is actually equivalent to a general quantum spin-1 chain.

We identify the spin with the string *height difference*  $y_{l+1} - y_l$ , which can be either 0, 1 or -1, see Fig. 10.

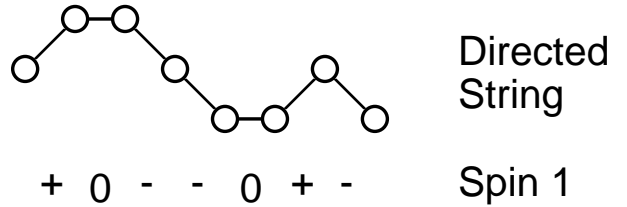


FIG. 10. The relation between spin-1 and directed strings,  $S_l^z = y_{l+1} - y_l$ .

These link dynamical variables specifying the string can be directly identified with the  $m_s = 0, \pm 1$  variables of the spins living on the sites of the spin chain. Defining the latter using hard core bosons  $b_{m_s}^\dagger$ , the spin operators for the  $S = 1$  case become  $S^z = b_1^\dagger b_1 - b_{-1}^\dagger b_{-1}$ ,  $S^+ = \sqrt{2}(b_1^\dagger b_0 + b_0^\dagger b_{-1})$  and by comparing the action of the spin- and string operators on their respective Hilbert spaces one arrives at operator identities [26]. A quantum hop from  $y$  to  $y+1$  increases the height difference on the left of  $l$  by one, and decreases it by one on the right, as is easily seen by inspecting the two hopping terms in Fig. 2. Therefore [26],

$$S_l^z = y_{l+1} - y_l \\ S_{l-1}^\pm S_l^\mp = 2P_{Str}(y_l - y_{l-1})P_{Str}(y_{l+1} - y_l)e^{\pm i\hat{\pi}_l}. \quad (5.2)$$

The following identities, for  $S = 1$ ,

$$\begin{aligned} \delta(|y_{l+1} - y_l| - 1) &= (S_l^z)^2, \\ \delta(|y_{l+1} - y_{l-1}| - 1) &= (S_l^z)^2 + (S_{l-1}^z)^2 - 2(S_l^z S_{l-1}^z)^2, \\ \delta(|y_{l+1} - y_{l-1}| - 2) &= \frac{1}{2} S_l^z S_{l-1}^z [1 + S_l^z S_{l+1}^z], \end{aligned} \quad (5.3)$$

are easily checked. The directed string problem can now be reformulated in spin language as,

$$\begin{aligned} \mathcal{H}_{spin} = \sum_l \left[ & (\mathcal{K} + 2\mathcal{L}_{12})(S_l^z)^2 + \frac{\mathcal{L}_{22}}{2} S_l^z S_{l-1}^z \right. \\ & + \left( \frac{\mathcal{L}_{22}}{2} - 2\mathcal{L}_{12} \right) (S_l^z S_{l-1}^z)^2 \\ & \left. + \frac{\mathcal{T}}{2} (S_l^+ S_{l-1}^- + S_l^- S_{l-1}^+) \right]. \end{aligned} \quad (5.4)$$

Following the spin-1 literature we define the following parameters,

$$\begin{aligned} D &= \mathcal{K} + 2\mathcal{L}_{12}, \\ J &= \mathcal{L}_{12}/2, \\ E &= \mathcal{L}_{22}/2 - 2\mathcal{L}_{12}. \end{aligned} \quad (5.5)$$

The  $E$  term is new. It is a quartic Ising term, leading to extra phases and phase transitions. For the special choice  $E = 0$  ( $\mathcal{T} = 1$ ), the above Hamiltonian reduces to the familiar XXZ model with on-site anisotropy,

$$\begin{aligned} \mathcal{H}_{XXZ} = \sum_l \left[ & D(S_l^z)^2 + JS_l^z S_{l-1}^z \right. \\ & \left. + \frac{1}{2} (S_l^+ S_{l-1}^- + S_l^- S_{l-1}^+) \right]. \end{aligned} \quad (5.6)$$

The zero temperature phase diagram of the above spin-1 model has been discussed in detail in the literature. [38–41,26] In the next section we will briefly review the six phases found for this model, from a string perspective. Then we will show that a nonzero  $E$  parameter leads to the appearance of four extra phases in section VII.

Den Nijs and Rommelse [26] discuss a direct mapping between the spin chain and the RSOS surface. We stress that this mapping in fact involves two steps: First the RSOS model is mapped on a string problem, using the  $T$  matrix. Then the spins are identified as shown above. Thus the quantum string is a *natural intermediate* of the two other models. Den Nijs and Rommelse make use of the freedom in the choice of the  $T$  matrix to define a mapping which is slightly different from ours, since they introduce a transfer matrix along a diagonal, while we introduce one along the  $x$ -direction. As a result, in their case there are only interactions between next nearest neighbors along the  $(1, 1)$  direction, while our choice

allows for interactions between next nearest neighbors along the  $x$ -direction. Therefore, our RSOS model differs slightly from theirs.

The RSOS representation is more transparent than the quantum model. The spin-1 phases and the nature of the phase transitions all have a natural interpretation in space-time. For instance the Haldane phase, or AKLT wavefunction, with its mysterious hidden string order parameter is identified as a “disordered flat” RSOS surface [26] with a simple local order parameter. The height representation, dual to the spins, gives a similar local order parameter for the quantum string.

## VI. THE PHASES (E=0)

In this section the general string Hamiltonian will be simplified by leaving out the quartic Ising term ( $E = 0$  in Eqs. (5.4) and (5.5)). Our string problem is now equal to the spin-1 XXZ model. The zero-temperature phase diagram of the string problem is surprisingly rich, and even for the case  $E = 0$  there are 6 phases and a large variety of phase transitions. These phases can be classified in three groups: classical strings localized in space, quantum rough strings of the free variety, and partly delocalized phases of which the disordered flat phase is a remarkable example. In this section we will briefly review the six phases as discussed in the literature on the spin-1 XXZ problem (5.6). The problem will be addressed from the quantum string perspective. For more details we refer to Ref. [26]. In the next section we will show that with a finite  $E > 0$  four additional phases are stabilized.

The phase diagram of the quantum string is shown in Fig. 11, as a function of  $D$  and  $J$ . We have used the XXZ model parameters, defined in Eq. (5.5), such that the phase diagram can be compared directly with the spin-1 literature [38–41] and in particular with Fig. 13 of Ref. [26]. We will introduce below the various order parameters that have been introduced in this reference to distinguish the six phases in this phase diagram. The relation between the more general ( $E \neq 0$ ) string and spin phases will be clarified in the next section.

There is first of all a horizontal and a diagonal string phase. In the diagonal phase I no quantum fluctuations are allowed, since, as shown in Fig. 3 a diagonal string does not couple to other states by  $\mathcal{H}_Q$ . This phase is stabilized by a large and negative  $\mathcal{L}_{22}$ , so that since  $E = 0$  also  $J = \mathcal{L}_{12}/2 = \mathcal{L}_{22}/8$  is large and negative. A suitable variable introduced to define order parameters, following Ref. [26], is the Ising spin variable  $\sigma_l = (-1)^{y_l}$ , which identifies whether a given height is in an even or odd layer. This underlying spin model can have “ferromagnetic” or antiferromagnetic” order, and so we introduce the corresponding order parameters [42]

$$\rho = \langle \sigma_l \rangle, \quad \rho_{stag} = \langle (-1)^l \sigma_l \rangle,$$

$$\rho_{str} = \langle \sigma_l (y_{l+1} - y_l) \rangle . \quad (6.1)$$

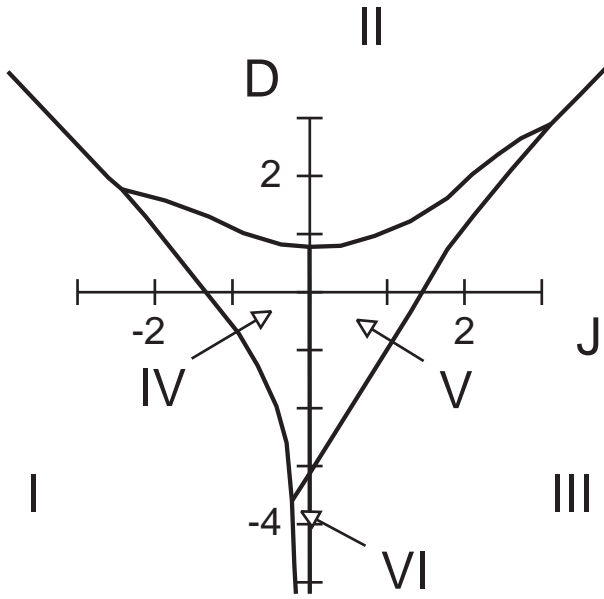


FIG. 11. The phases and phase transitions of the directed quantum string as a function of the on-site anisotropy  $D$  and the Ising interaction  $J$  of the corresponding spin-1 XXZ model. The parameter  $E$  is set to zero.

Here the brackets denote the ground state expectation value as well as an average over string members  $l$ . In (6.1), we have also included the order parameter  $\rho_{str}$  discussed below. In the horizontal phase II one particular height is favoured, thus the order parameter  $\rho$  is nonzero here. This phase is stabilized by a large positive  $\mathcal{K}$ , which suppresses diagonal links. However  $\mathcal{H}_Q$  causes virtual transitions from two horizontal links into two diagonal ones, see Fig. 2. On the 2D worldsheet these fluctuations show up as local terraces that do not overlap and thus do not destroy the long-range order. In both phases the elementary excitations are gapped.

Upon lowering  $\mathcal{K}$  the terraces grow and at some point they will form a percolated network — the string has become disordered in both space and imaginary time. Via the well-known Kosterlitz-Thouless roughening transition [35] phase IV is entered for  $J < 0$ . This phase belongs to the well known XY universality class, characterized by algebraic correlation functions and gapless meandering excitations — capillary waves in fluid interface language. The roughness, however, is extremely “soft” and the height difference diverges only logarithmically,  $\langle (y_l - y_m)^2 \rangle \sim \ln |l - m|$ . The transition from the Gaussian phase which is rough and on average oriented horizontally to the “frozen” diagonal phase is a “quasi first-order” KDP transition [26].

For large negative  $\mathcal{K}$  diagonal links are favored over horizontal ones. There is a transition to a second rough phase (phase VI). It is distinguished from the first by the

order parameter  $\rho_{stag}$ , which is zero in phase IV. In this phase horizontal links are virtual and occur in pairs. As we will discuss later in section VII, for large negative  $K$  the model can therefore be reduced to an effective spin 1/2 problem.

For negative  $\mathcal{K}$  and positive  $J$  ( $=\mathcal{L}_{12}/2 = \mathcal{L}_{22}/8$ ) the string becomes a (physically unlikely) zigzag with alternating up and down diagonal pieces. Excitations to pairs of horizontal links are gapped. Again  $\rho_{stag} = \langle (-1)^l \sigma_l \rangle$  serves as an order parameter. Upon increasing  $\mathcal{K}$  the islands formed by pairs of horizontal links start to overlap and there is an Ising transition into the Haldane or disordered flat (DOF) phase.

The point  $J = 1, D = 0$  belongs to the gapped DOF phase, in agreement with Haldane’s educated guess [43,44] that integer spin chains are gapped at the Heisenberg antiferromagnetic point. In this “disordered horizontal” string phase the prototype wavefunction, equal to the AKLT valence bond state [45], has every up diagonal link followed by a down link, with a random number of horizontal links in between. The height  $y_l$  takes just two values, say 0 and 1. The local order parameter is,  $\rho_{str}$ , defined in (6.1). This order parameter measures the correlation between the next step direction and whether one is in a layer of even or odd height. When  $\rho_{str} = 1$ , the string just steps up and down between two layers, but the steps can occur at arbitrary positions. Note that the height is a global quantity in spin language, i.e., it is the accumulated sum over spins,  $y_l = \sum_{m=0}^l S_m^z$ . Because of this the above order parameter becomes non-local when rewritten in terms of the “string” of spins. Therefore, it is often called the string order parameter. We will also use this name, but stress that the “string of spins” to which this name refers should not be confused with the general strings which are the basis of our model, and that the other order parameters are nonlocal as well in terms of the original spins  $S$ .

This phase diagram can be rationalized by writing the RSOS problem as the product of a 6-vertex model and the 2D Ising model of  $s$  spins on the 6-vertex lattice, as discussed in detail by Den Nijs and Rommelse. [26]. The horizontal, diagonal, zigzag but also the second rough phase VI all correspond to Ising order:  $\rho = \langle \sigma_l \rangle$  is nonzero in the horizontal phase II, while  $\rho_{stag} = \langle (-1)^l \sigma_l \rangle$  is nonzero in the diagonal phase I, the zigzag phase III and the rough phase VI. The six-vertex part is defined on the crossing points of steps on the surface — see Fig. 12. This is a (sometimes highly) diluted set of points. The Ising degree of freedom disorders on the transition between the phases III and V, and between IV and VI, while the six-vertex part remains unchanged. Therefore these transitions are Ising like. Transitions I  $\rightarrow$  IV, I  $\rightarrow$  VI, IV  $\rightarrow$  V and III  $\rightarrow$  VI are related to the six-vertex part becoming critical, and these KDP and KT transitions are known from the quantum spin-1/2 chain. The transition II to IV is related to the famous

surface-roughening transition, of the Kosterlitz-Thouless type. [35,36] The subtle transition between phase II and V, is coined “preroughening transition” by den Nijs. It separates two gapped phases. At the transition the gap closes and the system is Gaussian, with varying exponents along the transition line. [38–41]

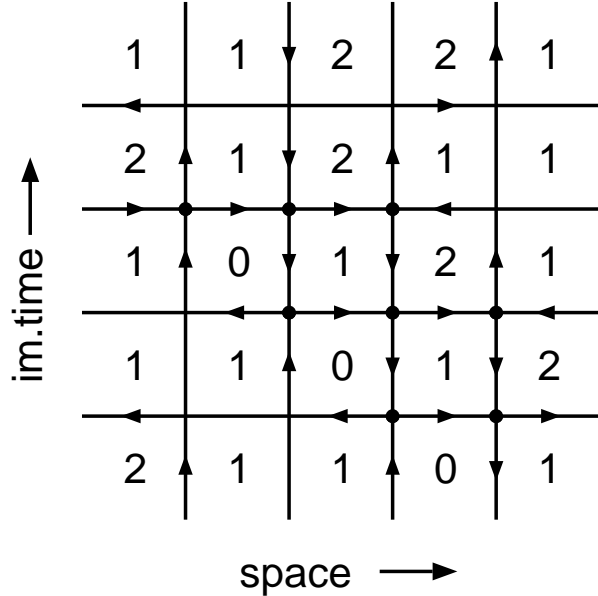


FIG. 12. Vertices (thick dots) on the space, imaginary time string worldsheet. The numbers correspond to the heights  $y_{l,k}$ . Arrows are drawn when the heights of neighbors differ. When four arrows occur at a crossing point this is called a vertex.

Almost all the phases can be distinguished by the above order parameters  $\rho$ ,  $\rho_{stag}$  and  $\rho_{str}$ , except that these do not discriminate between the diagonal phase I and the rough phase VI. These two phases can be identified by also introducing an order parameter which detects the presence of an average slope,  $\rho_{slope} = \langle y_{l+1} - y_l \rangle$ . In Table I we list the various phases for  $E = 0$  and the order parameters.

As we shall see in the next section, in the general case  $E \neq 0$  it is more convenient to introduce slightly different spin variables to identify all the ten different phases that occur then. The choice of Ref. [26] discussed here is somewhat more convenient for understanding the universality classes of the various phase transitions.

## VII. THE FULL PHASE DIAGRAM – PHASE-BOUNDARY ESTIMATES

As mentioned above the quartic Ising term with prefactor  $E$  generalizes the XXZ Hamiltonian and leads to extra phases. We will motivate that four extra phases are to be expected, and we will show that they are stabilized by a positive  $E$  parameter. The most disordered phase is still the Gaussian phase.

Using a similar decomposition as above, we can determine how many different phases to expect for a general spin-1 chain with  $z$ -axis anisotropy and nearest-neighbor interactions [46]. Think of the spin 1 as consisting of two spins  $\frac{1}{2}$ , see Table II. The first is  $\sigma^z = \downarrow$  when the spin 1 has  $S^z = 0$  and  $\sigma^z = \uparrow$  when  $S^z = \pm 1$ , similar to the Ising degree of freedom defined above. This spin thus indicates the presence or absence of a step. The second spin  $\frac{1}{2}$   $\mathbf{s}$ , is defined as  $s^z = S^z/2$  when  $S^z = \pm 1$  and is absent when  $S^z = 0$ . This is related to the diluted vertex network discussed by den Nijs and Rommelse, in that if there is a step, the  $z$ -component of  $\mathbf{s}$  indicates whether this step is up or down. The spins  $\mathbf{s}$  can have ferromagnetic (F) or antiferromagnetic (AF) order, or they can be disordered (D). For  $\sigma$  the two ferromagnetic cases correspond to different physical situations, and we have to distinguish ferromagnetic  $\downarrow$  (F1), a horizontal string, from ferromagnetic  $\uparrow$  (F2). When  $\sigma$  has F1 order,  $\mathbf{s}$  becomes irrelevant (or better — there are disconnected finite terraces of  $\mathbf{s}$  spins with short-range correlations). Therefore one expects 10 phases, depending on the order of the two spin species: 1 F1 phase, 3 F2 phases, 3  $\sigma$ -disordered phases, and 3  $\sigma$ -antiferromagnetically ordered phases. These are listed in Table III. An example of a phase diagram in a case in which all ten phases are present is shown in Fig. 13, which corresponds to the case  $E = 5$ . The detailed of how this phase diagram was obtained will be discussed below.

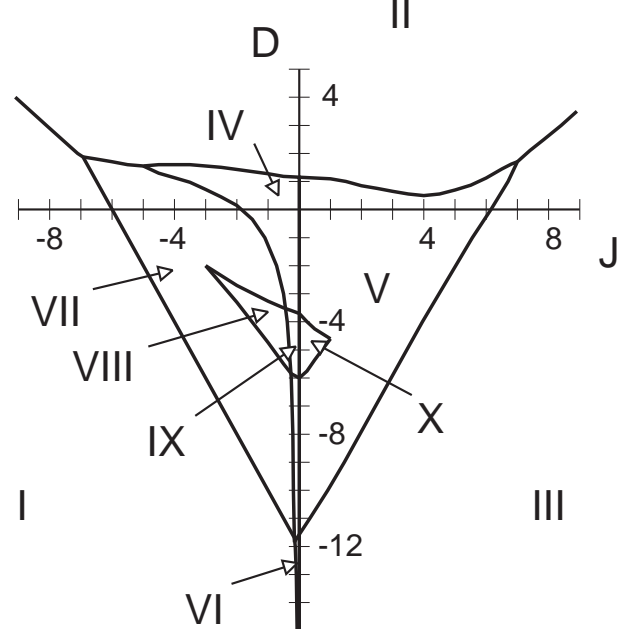


FIG. 13. The phases and phase transitions of the quantum string for  $E = 5$  as a function of  $t$ . On the axis are the on-site anisotropy  $D$  and the Ising interaction  $J$ .

There are four new phases, VII to X, compared to the phase diagram discussed in the previous section. All four are stabilized by a positive  $E$  parameter in Eq. (5.4). Three phases, VIII to X, result from an antiferromag-

netic order of the  $\sigma$  spin. This corresponds to alternating horizontal and diagonal string links (see Table III). The diagonal links can be either all up (FM, phase VIII), alternatingly up and down (AFM, phase X) or disordered (phase IX). In phase VII the  $\sigma$  spin is disordered, while the  $\mathbf{s}$  spin is in the FM phase. This is a diagonal wall diluted with horizontal links. These links coherently move up and down along the wall, lowering the kinetic energy. The wall can take any average angle between  $-\pi/4$  and  $\pi/4$ , and this angle is fixed by the value of the parameters. We will call this the “slanted” phase. In terms of the decomposition into an Ising spin model and a six-vertex model of den Nijs and Rommelse it is easy to see that the horizontal links change the orientation of the Ising spin and act like a Bloch wall. The Ising spin is therefore disordered. The six-vertex term is irrelevant for the existence of the slanted phase — in the case of a single horizontal link, i.e., on the boundary between the slanted and diagonal string phase, there are no vertices.

A large part of the phase boundaries can be estimated exactly, almost exactly, or to a fair approximation. Let us focus first on the classical phases. The diagonal, horizontal and zigzag phases have the following energies in the classical approximation in which there are no fluctuations, as is easily verified,

$$\begin{aligned} E_I &= L(\mathcal{K} + \mathcal{L}_{22}) = L(D + J + E), \\ E_{II} &\approx 0, \\ E_{III} &\approx L\mathcal{K} = L(D - J + E). \end{aligned} \quad (7.1)$$

where  $L$  is the length of the chain. The first-order transitions will therefore occur close to the lines  $\mathcal{K} = -\mathcal{L}_{22}$  ( $D = -J - E$ ) between phases I and II,  $\mathcal{L}_{22} = 0$  ( $J = 0$ ) between phases I and III, and  $\mathcal{K} = 0$  ( $D = J - E$ ) between phases II and III. These transitions become exact in the classical or large-spin limit.

The transition between phase I and VII, the diagonal and slanted phase, can be found exactly. The transition is of the Pokrovsky-Talapov, or conventional 1D metal-insulator type (see, for instance, Ref. [25]). The horizontal link can be seen as a hard-core particle or a spinless fermion, with the parameters determining an effective chemical potential. For a critical chemical potential equal to the bottom of the band of the hard-core particle the band will start to fill up. The transition occurs when the diagonal string becomes unstable with respect to a diagonal string with one horizontal link added. This single link delocalizes along the string with a momentum  $k$  and a kinetic energy  $2\mathcal{T} \cos(k)$ . The minimal energy is  $(L-1)\mathcal{K} + (L-2)\mathcal{L}_{22} + 2\mathcal{L}_{12} - 2\mathcal{T}$ , and the transition occurs when  $\mathcal{K} = 2(\mathcal{L}_{12} - \mathcal{L}_{22} - \mathcal{T})$  or, with  $\mathcal{T} = 1$ , when

$$\text{I to VII transition: } D = -2(J + E + 1). \quad (7.2)$$

The transition between phase III and V will occur when horizontal link pairs unbind in the zigzag background. A rough estimate, neglecting fluctuations, is

obtained by comparing the energy of a single horizontal link with that of a perfect zigzag. In the same way as above we estimate the phase boundary to be close to  $D = 2(J - E - 1)$ . In the same way the transition from phase II to V or IV is determined by the energy of a single diagonal step in a horizontal wall, which becomes favourable when  $D = 2$ . This last estimate turns out to be very crude, in that it largely underestimates the stability of the flat phase.

For large negative  $\mathcal{K}$  the horizontal links are strongly suppressed, and the string can be mapped perturbatively on a spin 1/2 chain. Identify  $S^z = 1$  (diagonal upward) with  $s^z = \uparrow$  and  $S^z = -1$  (diagonal downward) with  $s^z = \downarrow$ . Via a virtual (0,0) spin pair (two horizontal links) the spins can still fluctuate,  $(1,-1) \rightarrow (0,0) \rightarrow (-1,1)$ . One finds, using second-order perturbation theory in  $\mathcal{T}/\mathcal{K}$ ,

$$\begin{aligned} \mathcal{H}_{eff}(D \rightarrow -\infty) &= (4J + j_{\pm}) \sum_l s_l^z s_{l+1}^z \\ &\quad + j_{\pm} \frac{1}{2} \sum_l (s_l^+ s_{l+1}^- + s_l^- s_{l+1}^+) , \\ j_{\pm} &= \frac{2\mathcal{T}^2}{|2D + 3E|}. \end{aligned} \quad (7.3)$$

Here we subtracted an irrelevant constant term. This has the form of the well studied spin 1/2 Heisenberg chain with Ising anisotropy. Transitions occur when  $(4J + j_{\pm}) = \pm j_{\pm}$ , or when  $J = 0$  (III to VI) and  $J = -1/|2D + 3E|$  (I to VI) (setting  $\mathcal{T} = 1$ ).

The above estimates seem to suggest that the line  $J = 0$  is special. Our numerical results show that it describes accurately the transition between III and VI, but also the transition between IV and V. This agrees with the arguments given by Den Nijs and Rommelse [26] that the Kosterlitz-Thouless transition between IV and V should occur precisely at the  $J = 0$  line.

The slanted phase consists predominantly of up diagonal and horizontal links. Neglecting down diagonals altogether, which turns out to be a good approximation, one can again map the string or spin-1 chain on an effective spin 1/2 system. Now the relevant degree of freedom is the  $\sigma$  Ising degree of freedom. Because  $\sigma = \uparrow$  (a diagonal link) is not symmetrically equivalent to  $\sigma = \downarrow$  (a horizontal link) the spins will feel an effective magnetic field, which regulates the density of horizontal links. Rewriting Eq. (5.4) gives,

$$\begin{aligned} \mathcal{H}_{eff} &= D \sum_l (\sigma_l^z + \frac{1}{2}) \\ &\quad + (J + E) \sum_l (\sigma_l^z + \frac{1}{2})(\sigma_{l+1}^z + \frac{1}{2}) \\ &\quad + \mathcal{T} \sum_l (\sigma_l^+ \sigma_{l+1}^- + \sigma_l^- \sigma_{l+1}^+), \end{aligned} \quad (7.4)$$

and, after rescaling and putting  $\mathcal{T} = 1$ ,

$$\mathcal{H}_{eff} = h \sum_l \sigma_l^z + \Delta \sum_l \sigma_l^z \sigma_{l+1}^z + \frac{1}{2} \sum_l (\sigma_l^+ \sigma_{l+1}^- + \sigma_l^- \sigma_{l+1}^+) , \quad (7.5)$$

with the field  $h = (D + J + E)/2$  and Ising coupling  $\Delta = (J + E)/2$ . On the line  $h = 0$  the number of up diagonal links equals the number of horizontal links. The average tilt angle is thus  $22.5^\circ$  in this approximation. The phase diagram of the spin 1/2 chain in the  $h$ - $\Delta$  plane was discussed by Johnson and McCoy [47]. For  $h = 0$  there are three phases. The ferromagnet corresponds to phase I, the antiferromagnet with phase VIII, and the gapless disordered phase translates to the slanted string phase VII. Increasing the field  $h$  in the AFM phase will cause a transition to the gapless phase with a finite magnetization. In the approximation that down diagonals are neglected, it follows from the results of Johnson and McCoy [47] that the point  $\Delta = 1, h = 0$  or  $J = 2 - E$  is the point with the most negative value of  $J$  where phase VIII is stable. For  $E = 0$  (as well as for small values of  $E$ ) this occurs in the positive  $J$  side of the phase diagram, meaning that phase VIII to X will in fact not be stable: for positive values of  $J$ , down steps in the original model proliferate. To have a phase diagram with all 10 phases present we choose  $E = 5$ .

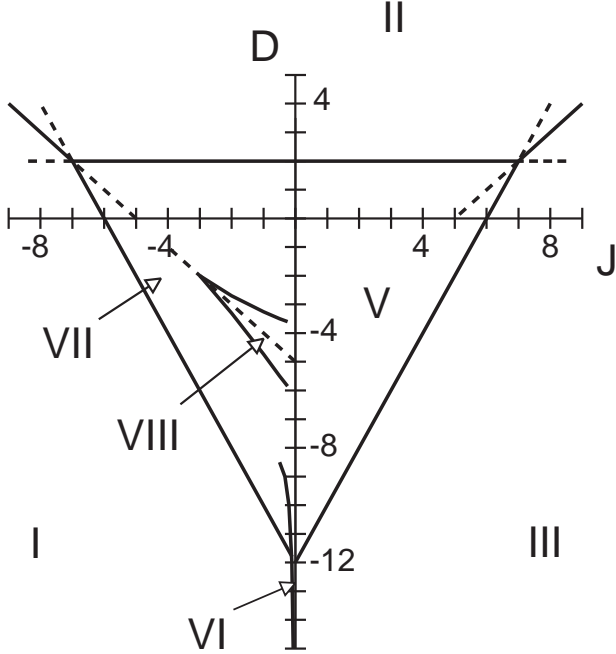


FIG. 14. The various phase transitions, obtained from semiclassical estimates, exact arguments and perturbative mappings to spin 1/2.

In Fig. 14 the various phase-boundary estimates given above are summarized. The topology of the main part of the phase-diagram has now become clear. In the centre of the figure for  $E = 5$  the Johnson-McCoy phase diagram is inserted. The estimates suggest that at least phase VII

and VIII are stabilized by taking  $E = 5$ . The dotted line through phase VIII is the line where the effective field  $h$  is zero, and the number of diagonal links is (nearly) equal to the number of horizontal ones.

We finally argue that the slanted phase exists in some region of the phase diagram for any  $E > 0$ . To see this, first consider the case  $E = 0$ . Along the line  $D = 0$ , our model (with  $E = 0$ ) corresponds to the Heisenberg model with Ising anisotropy, and the point  $J = -1$  corresponds to the isotropic ferromagnetic Heisenberg point. Along the line  $D = 0$ , the transition from the “ferromagnetic” (diagonal in string language) phase I to the XY phase IV therefore occurs at  $J = -1$ . Now, for  $E = 0$ , the exact location of the line along which phase I becomes unstable to the slanted phase VII, given by  $D = -2(J + 1)$  according to (7.2), goes exactly through the ferromagnetic Heisenberg point at  $J = -1$  as well. The results of Fig. 13 of den Nijs and Rommelse [26] indicate that this line then touches the phase boundary between phases I and IV right at this point in such a way that for  $E = 0$  no slanted phase occurs. If we assume that both phase boundaries shift linear in  $E$  for  $E$  nonzero and small, it is clear that the slanted phase must stabilize in some region near the point  $D = 0, J = -1$  for one sign of  $E$ , while for the other sign the phase must be absent. Physically, it is clear that the stabilization of the slanted phase will occur for positive values of  $E$ ,  $E > 0$ .

## VIII. NUMERICAL

To fill in the details of the phase diagram we have performed exact diagonalization and finite-temperature quantum-Monte Carlo calculations. Ground state properties of strings up to 15 holes (spin chains of length 14) were obtained using the Lanczos diagonalization method. For the Monte-Carlo we used the checkerboard decomposition, briefly explained in Sec. III. The Monte Carlo has the disadvantage that an extra limit to zero temperature has to be taken, a regime where the updating slows down considerably and where it is difficult to judge the accuracy. For determining the phase boundaries of the directed string we mainly used the Lanczos results for the equivalent spin model. On the other hand the Monte Carlo space-time worldsheets provide a transparent physical insight into the phases, phase transitions, order parameters, etcetera. Moreover, the Monte Carlo method allows, of course, to treat bigger systems.

We are in the fortunate situation that the order parameters of the various phases and the universality classes of the transitions are known. This offers a variety of approaches to determine the critical lines — one can monitor the finite-size behavior of the order parameter, correlation functions or the energy level spacings. Typically we applied two independent methods to the various

transitions. Our aim is to map out the entire phase diagram with an accuracy of roughly the line thickness in the phase diagram. For very accurate estimates other methods, notably the density-matrix renormalization group treatment of White [48], are more appropriate.

An elegant and powerful method is the phenomenological renormalization group approach pioneered by Nightingale. [49,50] In this approach one considers an infinite strip with a width  $L$ , as a finite-size approximation to the 2D classical system. At the critical temperature of the infinite system one expects, from finite size scaling, that the correlation length along the strip scales like the width of the strip ( $L_1$  or  $L_2$ ),

$$\xi_{L_1}(T_c) = \frac{L_1}{L_2} \xi_{L_2}(T_c). \quad (8.1)$$

The infinite strip is solved by diagonalizing the (finite)  $T$  matrix. The correlation length can be calculated from,

$$\xi = 1/\ln(\lambda_1/\lambda_0), \quad (8.2)$$

where  $\lambda_0$  and  $\lambda_1$  are the largest and second largest eigenvalues of the  $T$  matrix.

A finite 1D quantum chain can be viewed as a strip infinitely long in the imaginary time direction (zero temperature). In the time continuum limit, writing  $T = \exp(\tau H)$ , the equation corresponding to Eqs. (8.1) and (8.2) is,

$$L_1[E_1(L_1) - E_0(L_1)] = L_2[E_1(L_2) - E_0(L_2)], \quad (8.3)$$

for two different string lengths  $L_1, L_2 \rightarrow \infty$  and for parameter values at criticality. Here  $E_0$  and  $E_1$  are the ground state and first excited energy of a quantum Hamiltonian  $H$ . According to (8.3), a phase transition line can be located by studying the energy gap as a function of  $L$ , while monitoring when (8.3) is obeyed. A practical example of Eq. (8.3) is shown in Fig. 15. Successive curves for lengths  $L$  and  $L + 2$  show two crossing points. Extrapolating these crossing points to infinite  $L$  gives two estimates of the preroughening transition from phase II to V.

The above scaling holds when time and space scale in the same way, or  $(E_1(q) - E_0) \sim q^z$ , with a dynamical exponent  $z = 1$ . This can be checked independently, giving a self-consistent justification of the use of Eq. (8.3). In a similar spirit one can determine the critical scaling of correlation functions of an operator  $O$  by monitoring the lowest energy state with a nonzero overlap with  $O|0\rangle$ . This has been used extensively [38–41] to study the phases and exponents of the Gaussian phases of the spin-1 chain. We refer to these articles for more details.

Another method used to determine second-order phase transitions is the Binder parameter [51], which we define as  $(3 - \langle m^4 \rangle / \langle m^2 \rangle^2) / 2$ , where  $m$  is the relevant order parameter. This quantity tends to 1 in the ordered

phase, where  $\langle m^4 \rangle \approx \langle m \rangle^4$ , and approaches 0 in the disordered phase, where  $m$  has a Gaussian distribution around  $\langle m \rangle = 0$ . In a renormalization group sense the shape of the order parameter distribution function becomes independent of the size at criticality. The various curves for different sizes of the Binder parameter versus model parameters or  $T$  should therefore cross at the critical point. For instance for the Ising transition between phase III and V we take  $m = (-1)^{y_L - l}$ , the Ising degree of freedom introduced before.

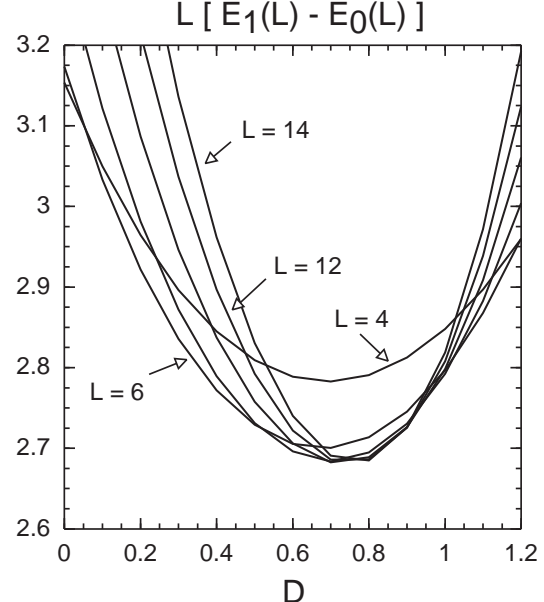


FIG. 15. Estimate of the preroughening transition between phase II and V. The plot shows  $L[E_1(L) - E_0(L)]$  for various lengths  $L$ , as a function of the parameter  $D$ , with  $J = 0.8$  and  $E = 0$ . The two crossing points between the successive curves form an upper and lower estimate of the transition.

The Kosterlitz-Thouless transition between for instance IV and V is a subtle one due to the infinite order of the transition and the exponential vanishing of the gap. Previous studies show a large uncertainty in the position of the transition line. In the entire Gaussian rough string phase the system is critical. Height correlations diverge very weakly like  $G(r) = \langle (y_r - y_0)^2 \rangle \propto C \ln(r)$ . At the KT transition point the prefactor takes the universal [36] value  $C = 2/\pi^2$ . We found that this relation is very useful to determine the KT transition line — see Fig. 16. This relation gives surprisingly good results even for very small distances, and is consistent with a KT transition at  $J = 0$ , as discussed by den Nijs and Rommelse. [26]

The phase diagram for  $E = 5$  is shown in Fig. 13. For this value of  $E$  the slanted phase VII is very pronounced. The phases VIII to X occur in a small region in the middle of the diagram around the line of equal probability of horizontal and diagonal links, in the approximation that the Hamiltonian can be mapped onto the spin 1/2 problem (7.5). The rough phases occur at small negative

values of  $J$ . Phases I, II, III, V, VIII and X are gapped.

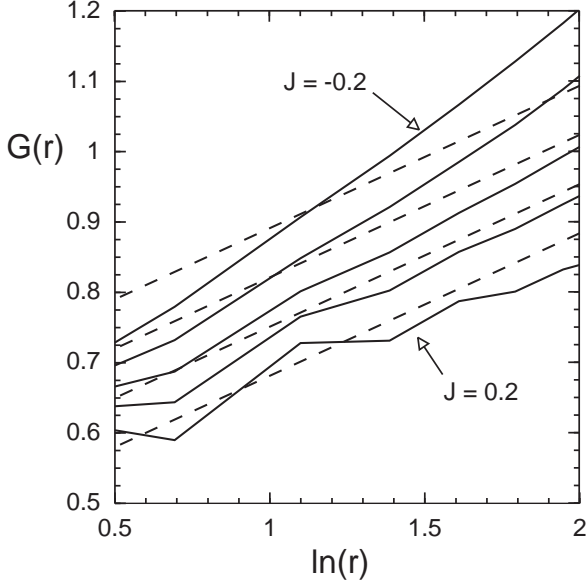
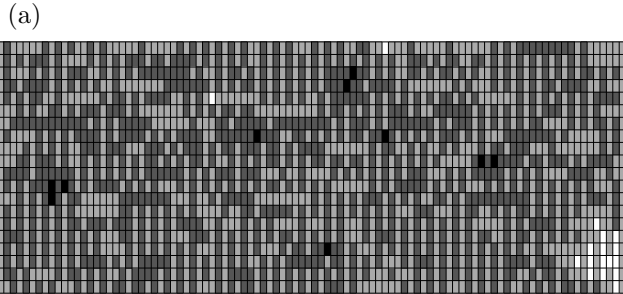


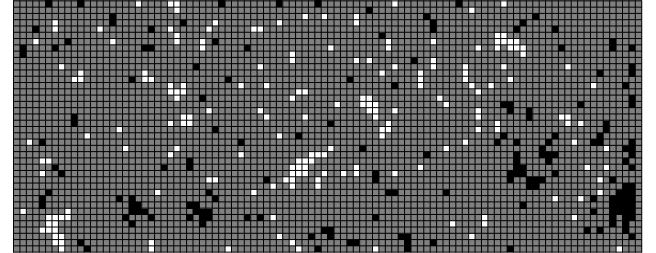
FIG. 16. Estimate of the Kosterlitz-Thouless transition between phase IV and V. At the transition the slope between  $G(r) = \langle (y_r - y_0)^2 \rangle$  and  $\ln(r)$  approaches  $2/\pi^2$  (the dotted lines).

The character of the various phases becomes clear by looking at the corresponding Monte-Carlo snapshots in Fig. 17.

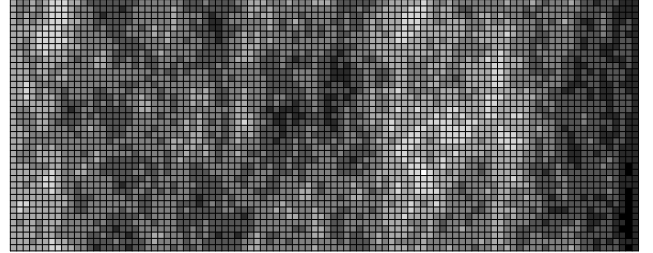
In the flat phase one particular height  $y_l$  dominates, and the quantum fluctuations do not percolate in space-time. Decreasing  $\mathcal{K}$  these quantum fluctuation islands grow and when they overlap the string enters phase IV. The system is Gaussian rough in both space and time. Note the very weak logarithmic meandering — e.g. for a string of length 10, Fig. 16 shows that the mean square height fluctuations are only of order 1 near the KT transition. Despite this, determining the KT transition from  $G(r)$  works surprisingly well for the small systems calculated.



(b)



(c)



(d)

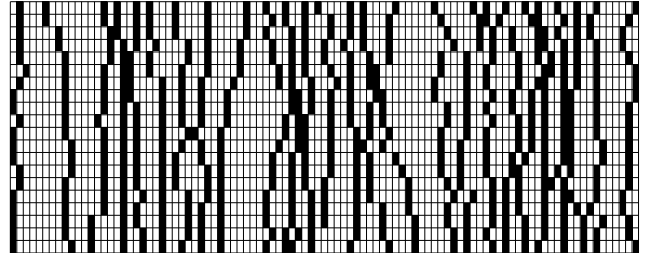


FIG. 17. Monte-Carlo snapshots of (a) the Haldane phase (Phase V,  $D = 0, J = 1, E = 0$ ), (b) the flat phase (Phase II,  $D = 2, J = 0, E = 0$ ), (c) the rough phase (Phase IV,  $D = 0, J = -0.5, E = 0$ ) and (d) the slanted phase (Phase VII,  $D = -0.75, J = -5, E = 5$ ). Black to white means increasing height, except for the slanted phase in (d), where black denotes a horizontal link and white an up diagonal link.

The fascinating order parameter of the Haldane phase or disordered flat phase becomes transparent when looking at the worldsheet, using the height representation instead of the spin-1 language. Globally the surface is limited to two heights only, and is therefore macroscopically flat. However in both the time and space direction there is a disordered array of up and down steps, with the restriction that every step up is followed by a step down, when the order is perfect. On flat pieces, however, there are local fluctuations (with consecutive up steps or down steps) decreasing the value of the order parameter. These islands will grow when  $J \rightarrow 0$  from the positive side, and when they overlap the string becomes rough. Note that the rigidity (flatness) is clear when viewing the overall structure of the worldsheet in 1+1D. On the other hand, from a single time slice one might be tempted to conclude that the string is rough.

The transition from phase I to VII is of the Prokovsky-

Talapov type. Such transitions are often discussed in the context of commensurate-incommensurate transition of a monolayer of atoms on a substrate with a different lattice parameter. In the “floating solid” phase such a system consists of a set of parallel domain walls with entropic meandering. [25] The similarity with phase VII, illustrated in Fig. 17 is clear. The entropic meandering in the 2D classical case is now to be interpreted as the quantum motion of hard-core particles (horizontal links) along the string.

## IX. DISCUSSION AND CONCLUSIONS

Motivated by stripes, we have introduced a lattice string model for quantum domain walls and mapped out its full phase diagram. We find a generic zero temperature symmetry breaking: the string acquires a direction in all cases. The main reason is that bends in the string prohibit the quantum transport, or, vice versa, the quantum motion of kinks straightens out the string (the “garden hose” effect of Nayak and Wilczek [12]). We arrive at the counter-intuitive conclusion that for increasing kink quantum disorder the orientational preference of the string grows. The directed string problem which remains appears to be related to a well understood surface statistical physics (RSOS) model and simultaneously to a  $S = 1$  XXZ quantum spin chain with single site anisotropy. Motivated by the string interpretation, we found a number of phases described by this class of models which were previously not identified.

Physically, the phases fall in three main categories: classical (flat worldsheet), Gaussian (rough worldsheet) and ‘disordered flat’ phases. The phases are further distinguished by the direction they take in the embedding space. Besides the flat strings in the horizontal and diagonal directions, we find that the disordered flat phases show here a rich behavior. Apart from the known phase with horizontal direction, which is associated with the incompressible phase of the spin model, we identified a new category of disordered flat phases which take, depending on parameters, arbitrary directions in space (the “slanted” phases).

Although this does not apply to the localized strings, we suspect that a strong universality principle might apply to the delocalized strings: *At least away from the phase boundaries to the localized phases, the underlying lattice renders the delocalized strings to be described by free field theory.* The reason is simple: *regardless of the terms that one adds to the lattice scale action, the problem remains of the XXZ kind and the massless phases fall into the 1+1D  $O(2)$  universality class.* For instance, one can add other kink-kink interactions, etcetera, and these can be all described by products of  $S^z$  operators. Although these operators determine the nature of the localized phases, they turn into irrelevant operators in the

massless phases. The kinetic sector is more subtle. For instance, one would like to release the constraint that kinks only occur with ‘height flavor’  $\pm 1$ . This means in surface language that one partially lifts the restrictedness of the RSOS model, or in spin language that one *increases the total spin*: e.g.,  $S = 2$  means in string language that kinks occur describing height differences of  $\pm 2$  as well. Although increasing the magnitude of spin has an influence on the localized phases, it does not change the fact that the massless phase away from the phase boundaries is still obeying XY universality. A point of caution is that the ‘holes’ in principle could change their order when larger excursions are allowed. However, these ‘exchange loops’ are strictly local and therefore irrelevant for the long wavelength behavior as long as the string is internally an insulator. These could represent more of a problem for strings which are internally superconductors or metals.

We also stress that it follows from the arguments of den Nijs and Rommelse [26] that the occurrence of a gapped Haldane type phase for strings is not a peculiar feature of the spin 1 representation, but a general consequence of the existence of further neighbor interactions between the holes in strings.

Do our findings bear any relevance to the stripes in cuprates? At the very least, they do bring up some interesting questions:

(a) Is the stripe solidification in for instance the LTT cuprates [3] in first instance driven by a single string effect or by a collective transition of the string liquid? In the end it has to be the latter, since a single string cannot undergo phase transitions at finite temperatures. However, it can be well imagined that the effect of the LTT-pinning potential is to stabilize  $(1,0)$  directed stripes over  $(1,1)$  stripes. In the language of this paper, this amounts to an increase of the parameter  $K$  which could move the stripe from the Gaussian phase into the horizontal flat phase. At zero temperature, this would turn individual stripes in straight rods which are obviously much easier to order than meandering strings. At finite temperatures, this could increase the single string persistence length substantially, so that stripe-stripe interactions become more effective in stabilizing a stripe solid at finite temperatures [52]. Further work is needed to establish if these single stripe transitions are of relevance.

(b) Do the ‘disordered flat’ string phases exist? The simplest disordered flat phase is the horizontal one (phase V) corresponding with the Haldane phase of the  $S = 1$  spin chain. In string language, this is nothing else than a localized string along the  $(1,0)$  direction in the lattice which is however not site-centered (as phase II) but, on average, *bond centered*. Bond centered stripes show up in the numerical study of the  $t$ - $J$  model by White and Scalapino [19], which shows that the ground state of this model at finite dopings is a stripe phase. A main difference with the mean-field stripes is that these  $t$ - $J$  stripes are bond

centered. In first instance, one could be tempted to think that this has a truly microscopic reason: charges in  $t$ - $J$  prefer to live on links. However, it could also be due to a *collective string effect* — it could be “our” phase V. This can be easily established by measuring the appropriate (string) correlators. Is it so that on equal times the charges live on sites while the kinks take care of delocalizing the stripes over two lattice rows, or is it so that on all times the charges are living on the links? This is obviously an important question in the light of recent works relating the bond centering via Hubbard-ladder physics to superconductivity [22]. We also notice that there are experimental indications for bond-centering in the nickelates [53] where disordered flatness could possibly also play a role.

(c) If well developed stripes exist in the superconductors and/or metals, these have to occur in the form of a quantum disordered stripe phase, or a ‘quantum string liquid’. What is learnt in this regard from the present study of a single string? A prerequisite for the existence of a quantum string liquid is that a single string is delocalized. If our conjecture that a single critical string is described by free field theory turns out to be correct, this amounts to a considerable simplification. In Euclidean space time, the single free string worldsheet is like a Gaussian membrane and a system of strings becomes a system of interacting Gaussian membranes, embedded in 2+1 dimensions. This in turn is like a classical incommensurate system in 3D which, although barely studied, appears as a tractable problem. For instance, it is known that the 3D incommensurate solid melts at a finite temperature in all cases [54]. For the quantum case this means that the quantum-melting transition will occur at some finite value of the coupling constant, which in turn depends on the single string quantum fluctuation as well as string-string interaction effects. Investigations addressing this many string problem are in progress, profiting from the simple fluctuation behavior of a single string.

## ACKNOWLEDGMENTS

We thank S. A. Kivelson for stimulating discussions. The work of HE was supported by the Stichting voor Fundamenteel Onderzoek der Materie (FOM), which is financially supported by the Nederlandse Organisatie voor Wetenschappelijk Onderzoek (NWO), and JZ acknowledges support by the Dutch Royal Academy of Sciences (KNAW).

## APPENDIX.

In this appendix we give the  $t$ -matrix elements of the blocks defined in Fig. 3. The local  $t$ -matrix at position  $l$  and Trotter slice  $k$  is defined as,

$$\langle \mathbf{r}_{l-1,k}, \mathbf{r}_{l,k}, \mathbf{r}_{l+1,k} | \exp \frac{1}{n} \mathcal{H}_l | \mathbf{r}'_{l-1,k}, \mathbf{r}'_{l,k}, \mathbf{r}'_{l+1,k} \rangle. \quad (9.1)$$

The matrix elements depend on the positions of three members of the string,  $l - 1$ ,  $l$  and  $l + 1$ . The positions of  $l - 1$  and  $l + 1$  are required to be identical  $\mathbf{r}_{l-1,k} = \mathbf{r}'_{l-1,k} \mathbf{r}'_{l-1,k}$  in the two Trotter subslices involved, due to the checkerboard decomposition, but the position of member  $l$  can be different, leading to off-diagonal matrix elements. The matrix elements of the  $t$ -matrix are easily found by first diagonalizing  $\mathcal{H}_\uparrow$  and expanding the basis vectors in terms of the eigenvectors.

Block A: This block contains three configurations, see Fig. 3. We use the same order for the states as in the figure. Note that only half of the energy  $\mathcal{K}$  of the diagonal link between  $l - 1$  and  $l$  and the link between  $l$  and  $l + 1$  should be contributed to  $l$ . The Hamiltonian,

$$\mathcal{H} = \begin{pmatrix} \mathcal{K} & \mathcal{T} & 0 \\ \mathcal{T} & 0 & \mathcal{T} \\ 0 & \mathcal{T} & \mathcal{K} \end{pmatrix}, \quad (9.2)$$

is easily diagonalized. The eigenvalues are  $\mathcal{K}$ ,  $E_+$  and  $E_-$ . The  $t$ -matrix is,

$$\begin{aligned} t &= \begin{pmatrix} t_{11} & t_{12} & t_{13} \\ t_{12} & t_{22} & t_{12} \\ t_{13} & t_{12} & T_{11} \end{pmatrix}, \\ t_{11} &= \frac{1}{2} e^{\mathcal{K}/n} + N_+^2 e^{E_+/n} + N_-^2 e^{E_-/n}, \\ t_{12} &= N_+^2 \alpha_+ e^{E_+/n} + N_-^2 \alpha_- e^{E_-/n}, \\ t_{13} &= -\frac{1}{2} e^{\mathcal{K}/n} + N_+^2 e^{E_+/n} + N_-^2 e^{E_-/n}, \\ t_{22} &= N_+^2 \alpha_+^2 e^{E_+/n} + N_-^2 e^{E_-/n}, \\ E_\pm &= \frac{1}{2} \pm \frac{\sqrt{\mathcal{K}^2 + 8\mathcal{T}^2}}{2}, \\ \alpha_\pm &= \frac{E_\pm - \mathcal{K}}{\mathcal{T}}, \quad N_\pm = \frac{1}{\sqrt{2 + \alpha_\pm^2}}. \end{aligned} \quad (9.3)$$

Here  $n$  is the number of Trotter slices and  $\mathcal{K}$ ,  $\mathcal{L}_{12}$ ,  $\mathcal{L}_{22}$ ,  $\mathcal{L}_{11}$  and  $\mathcal{T}$  are the string model parameters.

Block B contains two configurations, each with one horizontal and one diagonal link. Repeating the above procedure one finds,

$$\begin{aligned} t &= \begin{pmatrix} e^D \cosh(\mathcal{T}/n) & e^D \sinh(\mathcal{T}/n) \\ e^D \sinh(\mathcal{T}/n) & e^D \cosh(\mathcal{T}/n) \end{pmatrix}, \\ D &= \frac{\mathcal{K}}{2n} + \frac{\mathcal{L}_{12}}{n} \end{aligned} \quad (9.4)$$

Block C contains a single configuration of two diagonal links, and the energy and  $t$ -matrix therefore contain  $\mathcal{L}_{22}$ ,

$$t = \exp\left(\frac{\mathcal{K}}{n} + \frac{\mathcal{L}_{22}}{n}\right), \quad (9.5)$$

Block D consists of a square corner between one horizontal and one vertical link, and  $\mathcal{L}_{11}$  is involved,

$$t = \exp\left(\frac{\mathcal{L}_{11}}{n}\right), \quad (9.6)$$

\* Present address: KNMI, Postbus 201, 3730 AE De Bilt, The Netherlands

- [1] See, e.g., B. G. Levi, Physics Today **49** (6) 17 (1996) and references therein.
- [2] Y. Ando, G. S. Boebinger, A. Passner, T. Kimura and K. Kishio, Phys. Rev. Lett. **75**, 4662 (1995); Y. Ando, G. S. Boebinger, A. Passner, N. L. Wang, C. Geiberl and F. Steglich, Phys. Rev. Lett. **77**, 2065 (1996); Y. Ando, G. S. Boebinger, A. Passner, T. Kimura, M. Okuya, J. Shimoyama, K. Kishio, K. Tamasaku, N. Ichikawa and S. Uchida, Phys. Rev. Lett. **77**, 5417 (1996).
- [3] J. M. Tranquada, B. J. Sternlieb, J. D. Axe, Y. Nakamura and S. Uchida, Nature **375** 561 (1995); see also J. M. Tranquada, condmat 9709325.
- [4] J. M. Tranquada, J. D. Axe, N. Ichikawa, A. R. Moodenbaugh, Y. Yakamura and S. Uchida, Phys. Rev. Lett. **78**, 338 (1997).
- [5] K. Yamada *et al.*, Physica C, in press.
- [6] K. Yamada *et al.*, *Doping dependence of spatially modulated dynamical spin correlations in superconducting  $La_{2-x}Sr_xCuO_4$* , Tohoku Univ. preprint (unpublished 1997).
- [7] J. M. Tranquada, *Charge stripes and spin correlations in copper-oxide superconductors*, cond-mat/9706261 (Physica C, in press).
- [8] P. Dai, H. A. Mook and F. Dogan, *Incommensurate magnetic fluctuations in  $YBa_2Cu_3O_{6.6}$* , cond-mat/9707112 (1997).
- [9] J. Zaanen, M.L. Horbach, and W. van Saarloos, Phys. Rev. B **53**, 8671 (1996).
- [10] D. M. Ceperley, Rev. Mod. Phys. **67**, 279 (1995).
- [11] H. Eskes, R. Grimberg, W. van Saarloos and J. Zaanen, Phys. Rev. B **54**, 724 (1996).
- [12] C. Nayak and F. Wilczek, Int. J. Mod. Phys. **10**, 2125 (1996); Phys. Rev. Lett. **78**, 2465 (1997).
- [13] See, e.g., G. Forgacs, R. Lipowsky and Th. M. Nieuwenhuizen, in: *Phase transitions and critical phenomena* vol. 14, C. Domb and J. L. Lebowitz, eds. (Academic, New York, 1991), or *Structure and Dynamics of Membranes*, R. Lipowsky and E. Sackmann, eds. (North-Holland, Amsterdam, 1995).
- [14] J. Zaanen and O. Gunnarson, Phys. Rev. B**40**, 7391 (1989).
- [15] D. Poilblanc and T. M. Rice, Phys. Rev. B**39**, 9749 (1989); H. J. Schulz, Phys. Rev. Lett. **64**, 1445 (1990); M. Kato *et al.*, J. Phys. Soc. Jpn. **59**, 1047 (1990); M. Inui and P. B. Littlewood, Phys. Rev. B **44**, 4415 (1991); J.A. Vergés, F. Guinea and E. Louis, Phys. Rev. B**46**, 3562 (1992); T. Giamarchi and C. Lhuillier, Phys. Rev. B **43**, 12943 (1991); G. An and J. M. J. van Leeuwen, Phys. Rev. **44**, 9410 (1991); H.J.M. van Bemmelen *et al.*, Phys. Rev. Lett. **72**, 2442 (1994); J. Zaanen and P.B. Littlewood, Phys. Rev B **50**, 7222 (1994).
- [16] U. Löw, V. J. Emery, K. Fabricius, and S. A. Kivelson, Phys. Rev. Lett. **72**, 1918 (1994); V. J. Emery and S. Kivelson, Physica C **209**, 597 (1993); S. A. Kivelson and V. J. Emery, Synth. Met. **80**, 151 (1996).
- [17] P. Prelovsek and X. Zotos, Phys. Rev B**47**, 5984 (1993); P. Prelovsek and I. Sega, Phys. Rev B**49**, 15241 (1994).
- [18] J. Zaanen and A.M. Oleś, Ann. Physik **5**, 224 (1996).
- [19] S. R. White and D. J. Scalapino, *DMRG study of the striped phase in the 2D t-J model*, cond-mat/9705128 (1997).
- [20] V. J. Emery, S. A. Kivelson and O. Zachar, *Spin-gap proximity effect mechanism of high temperature superconductivity*, cond-mat/9610094 (1996); A. H. Castro Neto, *Luttinger stripes in antiferromagnets*, cond-mat/9611146 (Z. Phys. B, in press, 1997); *ibid.*, cond-mat/9702180 (Phys. Rev. Lett., in press, 1997); A. H. Castro Neto, C. de C. Chamon and C. Nayak, *Open luttinger liquids*, cond-mat/9704120 (1997).
- [21] J. Zaanen, O. Y. Osman, H. Eskes and W. van Saarloos, J. Low Temp. Phys. **105**, 569 (1996).
- [22] Yu. A. Krotov, D.-H. Lee and A. V. Balatsky, *Superconductivity of a metallic stripe embedded in an antiferromagnet*, cond-mat/9705031 (1997).
- [23] J. Zaanen, O.Y. Osman, H. Eskes and W. van Saarloos, unpublished.
- [24] See, e.g., R. Rajaraman, *An Introduction to Solitons and Instantons in Quantum Field Theory* (North-Holland, Amsterdam, 1989).
- [25] M. den Nijs, in *Phase Transitions and Critical Phenomena*, Vol.12, Eds. C. Domb and J.L. Lebowitz, Academic Press, London, 1988.
- [26] M. den Nijs and K. Rommelse, Phys. Rev. B **40**, 4709 (1989).
- [27] V. Sachan *et al.*, Phys. Rev. B **51**, 12742 (1995); K. Nagaoka *et al.*, J. Phys. Soc. Jpn. **66**, 809 (1997).
- [28] S. R. White and D. J. Scalapino,  *$d_{x^2-y^2}$  pair domain walls*, cond-mat/9610104 (1996).
- [29] H.E. Viertö and T.M. Rice, J. Phys.: Condens. Matter **6**, 7091 (1994).
- [30] A. J. Heeger, S. Kivelson, J. R. Schrieffer and W.-P. Su, Rev. Mod. Phys. **60**, 781 (1988).
- [31] S. A. Brazovski, Zh. Eksp. Teor. Fiz. **78**, 677 (1980) [Sov. Phys. JETP **51**, 342 (1980)].
- [32] F. D. M. Haldane, Phys. Rev. Lett.
- [33] M. Suzuki, Progr. Theor. Phys. **56**, 1454 (1976).
- [34] J. D. Weeks, J. Chem. Phys. **67**, 3106 (1977); J. D. Weeks, Phys. Rev. Lett. **52**, 2160 (1984).
- [35] J. D. Weeks, in *Ordering in Strongly Fluctuating Condensed Matter Systems*, edited by T. Riste, Plenum, New York, 1980, p. 293.
- [36] H. van Beijeren and I. Nolten, in: *Structure and Dy-*

*Dynamics of Surfaces II*, eds. W. Schommers and P. von Blanckenhagen (Springer, Berlin, 1987).

[37] In the high temperature limit, the string becomes a self-avoiding walk on a two-dimensional lattice. For such a walk of length  $N$ , the radius of gyration  $R_g$  grows as  $R_g \sim N^\nu$  where  $\nu = 0.6$  in D=2. This implies that the directedness defined in this paper should go to zero as  $N^{\nu-1} = N^{-0.4}$  for  $N \rightarrow \infty$  in the high temperature limit.

[38] R. Botet, R. Jullien, and M. Kolb, Phys. Rev. B **28**, 3914 (1983).

[39] U. Glaes and T. Schneider, Phys. Rev. B **30**, 215 (1984).

[40] H. J. Schulz and T. Ziman, Phys. Rev. B **33**, 6545 (1986).

[41] H. J. Schulz, Phys. Rev. B **34**, 6372 (1986).

[42] These order parameters, as well as the string order parameter introduced below, are only nonzero once the height at an arbitrary point is specified. This can, e.g., be the guider point discussed in section V or the reference height  $h_0$  introduced in Ref. [26].

[43] F. D. M. Haldane, Phys. Rev. Lett. **50**, 1153 (1983).

[44] I. Affleck, J. Phys. Condens. Matter **1** 3047 (1989).

[45] I. Affleck, T. Kennedy, E. H. Lieb, and H. Tasaki, Phys. Rev. Lett. **59**, 799 (1987); Commun. Math. Phys. **115**, 477 (1988).

[46] U. Schollwöck and T. Jolicœur, Europh. Lett. **30**, 493 (1995).

[47] J. D. Johnson and B. M. McCoy, Phys. Rev. A **6**, 1613 (1972).

[48] S. R. White, Phys. Rev. Lett. **69**, 2863 (1992).

[49] P. Nightingale, J. Appl. Phys. **53**, 7927 (1982).

[50] M. N. Barber in *Phase Transitions and Critical Phenomena*, Vol.8, Eds. C. Domb and J.L. Lebowitz, Academic Press, London, 1983.

[51] K. Binder, Z. Phys. B - Condensed Matter **43**, 119 (1981).

[52] S. N. Coppersmith, D. S. Fisher, B. I. Halperin, P. A. Lee and W. F. Brinkman, Phys. Rev. B **25**, 349 (1982).

[53] J. M. Tranquada, D. J. Buttrey and V. Sachan, Phys. Rev. B **54**, 12318 (1996); Phys. Rev. B **55**, R6113 (1997); P. Wochner *et al*, *Neutron diffraction study of stripe order in  $La_2NiO_{4+\delta}$  with  $\delta = 2/15$* , cond-mat/9706261 (1997).

[54] M. E. Fisher and D. S. Fisher, Phys. Rev. B **25**, 3192 (1982).

TABLE I. Order parameters that distinguish between the six different phases in the phase diagram for  $E = 0$ . A + entry in the table indicates that the particular order parameter is nonzero.

Phase	$\rho$	$\rho_{stag}$	$\rho_{str}$	$\rho_{slope}$
I		+		+
II	+			
III		+	+	
IV				
V			+	
VI		+		

TABLE II. Spin 1  $S$  seen as a combination of two spins 1/2,  $\sigma$  and  $s$ .

$S$	1	0	-1
$\sigma$	$\uparrow$	$\downarrow$	$\uparrow$
$s$	$\uparrow$	-	$\downarrow$

TABLE III. A schematic representation of the different phases. Also shown is the long-range order of the two spins  $1/2$ ,  $s$  and  $\sigma$  as defined in the text. F = ferromagnetic, F1 = up-spin ferromagnetic, F2 = down-spin ferromagnetic, AF = antiferromagnetic, D = disordered

Phase	$\sigma$	s	String	Spin 1
I	F1	F	• . • .	++++++
II	F2	-	••••••••	0 0 0 0 0 0 0
III	F1	AF	••••••••••	+-+-+-+-
IV	D	D	•••••••••••	+0-+0+0-+
V	D	AF	••••••••••	-+0-0 0+-
VI	F1	D	••••••••••	+-+-+-+-
VII	D	F	• . • .	0+0++0+0 0
VIII	AF	F	• . • .	0+0+0+0+0
IX	AF	D	••••••••••	0+0+0-0+0
X	AF	AF	••••••••••	0+0-0+0-0